Taylor & Francis
Taylor & Francis Group

Spectroscopy Letters

An International Journal for Rapid Communication

ISSN: 0038-7010 (Print) 1532-2289 (Online) Journal homepage: www.tandfonline.com/journals/lstl20

Experimental and theoretical spectroscopic properties, antimicrobial activity, and molecular docking studies of methyl 6-quinolyl ether

Merve Nurhan Güney, Şenay Yurdakul & Belgin Erdem

To cite this article: Merve Nurhan Güney, Şenay Yurdakul & Belgin Erdem (10 Oct 2025): Experimental and theoretical spectroscopic properties, antimicrobial activity, and molecular docking studies of methyl 6-quinolyl ether, Spectroscopy Letters, DOI: 10.1080/00387010.2025.2569625

To link to this article: https://doi.org/10.1080/00387010.2025.2569625

SPECTROSCOPY LETTERS
https://doi.org/10.1080/00387010.2025.2569625

Taylor & Francis
Taylor & Francis Group

RESEARCH ARTICLE

Experimental and theoretical spectroscopic properties, antimicrobial activity, and molecular docking studies of methyl 6-quinolyl ether

Merve Nurhan Güney[a], Şenay Yurdakul[a] and Belgin Erdem[b]

[a]Department of Physics, Faculty of Science, Gazi University, Ankara, Turkey; [b]Department of Health Care Services, Ahi Evran University, Kırşehir, Turkey

ABSTRACT

In this study, we describe the structural characterization of methyl 6-quinolyl ether (M6-QE) molecule by Fourier Transform Infrared, Raman, and Nuclear Magnetic Resonance spectroscopic analysis. The molecular geometry of the title molecule was optimized by using density functional theory (DFT/B3LYP) with the 6–311++G(d,p) basis set. Molecular characteristics like highest occupied molecular orbital (HOMO)–lowest unoccupied molecular orbital (LUMO) energy, molecular electrostatic potential (MEP) distribution, atomic charges, Fukui, and electron localization functions (ELFs) are computed. Basic thermodynamic properties such as entropy, enthalpy changes, heat capacity, Gibbs free energy, and zero-point vibrational energy under constant pressure in the gas phase for different temperature values were also calculated. Further, nonlinear optical parameters such as dipole moment and linear and first-order hyperpolarizabilities of the title molecule have been studied. Infections caused by microorganisms resistant to antibiotics are still difficult to treat. The antimicrobial activity of M6-QE against pathogenic bacteria and yeast was also investigated in this study. M6-QE was determined to have quite potent antimicrobial activity against *B. subtilis* and *K. pneumoniae*. Moreover, this compound showed anti-quorum sensing (QS) activity in *C. violaceum* ATCC 12472. Also, the title molecule was docked into the reactive regions of protein structures of some microorganisms, and the docking minimum binding affinity values were given. Experiments have demonstrated that M6-QE inhibits harmful bacteria and stops QS, which makes the molecule a viable option for the creation of novel antimicrobial medications.

ARTICLE HISTORY
Received 27 August 2024
Accepted 28 September 2025

KEYWORDS
Antimicrobial activity; DFT; infrared and Raman Spectra; NMR

Introduction

Amongst heterocyclic compounds, especially quinoline and its derivatives, are advantaged in that they appear as significant assembly motifs for the development of devices such as sensors[1] and new drug entities.[2] It is known that the methoxy group plays an important role in the photophysics of quinoline and its derivatives. The photophysical properties of the methyl 6-quinolyl ether (M6-QE) have been explored, and they have been proposed as candidates for fluorescent probes, light-emitting devices, and optical thin-film sensors.[1,3–5] The sensor films are capable of determining aqueous halide in blood,[6] serum,[7] cheese,[8] and nuclear materials[9] in many areas of everyday life.

The quinoline ring system also occurs in various natural products, particularly in alkaloids, and is seldom used for a plan of many synthetic compounds with varied pharmacological properties. There are some natural products of the quinoline skeleton used as a drug or employed as lead molecules for the development of newer and persuasive molecules.[2] E.g., cinchona alkaloids are natural sources of quinolines that play important roles in medicine as antimalarial and antiarrhythmic drugs.[10,11]

The quinoline-based antibiotics ciprofloxacin and moxifloxacin, which are used for a number of bacterial infections, show significant antitubercular activity as well and are recommended by WHO as second-line anti-TB drugs. These quinoline drugs are also found to be good inhibitors of topoisomerase enzymes and prevent them from decatenating replicating DNA.[12,13] In this

CONTACT Şenay Yurdakul senayy@gazi.edu.tr Department of Physics, Faculty of Science, Gazi University, Ankara, Turkey.

perspective, the quinoline skeleton can be chosen for the design of new bioactive molecules.

An extensive literature survey reveals that no complete experimental spectroscopic studies and detailed density functional theory (DFT) calculations have been conducted yet for the M6-QE molecule. Therefore, the present aims to give detailed spectroscopic analysis, such as FT-IR, FT-Ra, and NMR (1H and 13C) studies, for the biologically important ligand. For this purpose, quantum chemical computations were carried out by using DFT/B3LYP at the level of 6–311++G(d,p). Other properties such as NBO, highest occupied molecular orbital (HOMO)–lowest unoccupied molecular orbital (LUMO), molecular electrostatic potential (MEP), Fukui functions, thermodynamic, and non-linear optical properties have been performed. According to literature review, it was determined that the newly synthesized molecule did not exhibit antimicrobial activity. However, recent studies on newly synthesized 2-azido-1H-benzod] imidazole molecules have shown significant antimicrobial activity against *S. aureus, E. coli, P. aeruginosa, A. niger*, *and C. albicans*.[14] In recent years infections caused by microorganisms resistant to antibiotics are still difficult to treat. In this study, the antimicrobial activity of M6-QE against pathogenic bacteria and yeast was also determined by the minimum inhibitory concentration (MIC) and the agar well diffusion method. The bacterial lines most sensitive to M6-QE were against *A. hydrophila, S .dysenteriae, S. aureus*, *K.pneumoniae, B. subtilis, C. albicans,* and *B. cereus* M6-QE molecule also showed good anti-quorum sensing (QS) activity against *C. violaceum* ATCC 12472. The title molecule was docked into the reactive regions of protein structures of some microorganisms, and the docking minimum binding affinity values were also given.

Procedure

Materials and methods

M6-QE was obtained from Sigma-Aldrich Chemical Company. This structure is offered for sale at 98% purity with the CAS number 5263-87-6. FT-IR and FT-Raman spectra were determined without further purification of the molecule. The FT-IR spectrum was recorded between 4000 and 400 cm^{-1} using a Bruker FT-IR spectrometer with ATR equipment. The FT-Raman spectrum was also recorded in the region of 4000–100 cm^{-1} using a Jasco FT-Raman spectrometer with an NRS400 confocal microscope. Chemical shifts of the title molecule for 1H and 13C NMR were recorded with the Bruker Ultrashield 300 MHz spectrometer.

Computational methods

Gaussian 09W[15] and GaussView 5.0.9[16] molecular visualization software packages were used for all theoretical calculations. Geometrical optimization and theoretical frequency calculations were made by DFT computations by using the Becke-3-Lee-Yang-Parr exchange correlation function[17,18] B3LYP and the 6–311++G(d,p) basis set.

The lowest energy level of the M6-QE molecule has been computed by evaluating the torsional potential energy as a function of the angle of rotation of the methyl group about the quinoline ring by using quantum chemical calculation.

Theoretical vibrational frequency values are multiplied by a certain multiplier factor and brought closer to the experimental values. This is called scaling. In this study, the theoretical frequency values with wavenumbers less than 1800 cm^{-1} were scaled by multiplying by 0.955, and those with wavenumbers greater than 1800 cm^{-1} by 0.997.[19,20]

For analyzing the non-bonded interactions, electron localization function (ELF) and localized orbital locator (LOL) also were performed by Multiwfn.[21]

The AutoDock Vina program[22] and the AutoDockTools graphical interface[23] were used for molecular docking research. The Protein Data Bank provided the 3D-dimensional crystal structure of the proteins.[24] The visualization can be accessed at the Discovery Studio Visualizer package program.[25]

Bacterial strains and growth conditions

The antimicrobial activity of M6-QE molecule was tested on nine reference bacterial strains (*E. coli* ATCC 25922, *P. aeruginosa* ATCC27853, *S. typhimurium* ATCC 14028, *S. dysenteriae* ATCC 11835, *A. hydrophila* ATCC 7966, *K. pneumoniae* ATCC13883, *S. aureus* ATCC25923, *B. cereus* 709 Roma, *B. subtilis* ATCC 6633), and one yeast strain (*C. albicans* ATCC 90028) was administered.

Test bacteria were routinely cultivated for 24 h at 37 °C on Tryptone Soy agar (TSA)/broth (Oxoid). Anti-QS activity was tested using a different reference strain, *C. violaceum* ATCC 12472.[26] TSA was used to plate the bacterial strains, and they were then incubated for 24–48 h at 37 °C. Sterile saline was used to suspend the developing colonies at a concentration of 1×10^6 CFU/mL.

Determination of minimum inhibitory concentration (MIC) and agar well diffusion

M6-QE molecule minimum inhibitory concentration (MIC) and agar well diffusion tests were performed according to CLSI[27] guidelines. M6-QE was dissolved in DMSO, and serial dilutions were made to reach final concentrations ranging from 512 to 16 µg/mL. An aliquot of 100 µL of bacterial suspension (1×10^6 CFU/mL) was inoculated into each well of a sterile 96-well microplate. The plates were incubated at 37 °C for 24 h. The MIC was the lowest concentration at which no microbial growth was observed.

In the agar well diffusion test, test bacteria and yeast ($1 \times$ CFU/mL) prepared at a concentration of 100 mg/mL were spread on the agar surface in a volume of 100 and 70 µL of M6-QE compound was dropped into the wells opened at 6 mm. The plates were incubated at 37 °C for 24 h. A digital caliper was used to measure the inhibition zones in millimeters. The negative control was DMSO, and the positive controls were Nystatin (100 U/mL) for *C. albicans* and Ampicillin (10 µg/mL) for bacteria. Each experiment was performed in triplicate.

Quorum-sensing inhibition assay

An agar diffusion method employing LB agar plates was used to examine the effect of M6-QE on violacein production by *C. violaceum* anti-QS property. On the agar surface, a 100 µL volume of freshly developed CV 12472 culture was dispersed, and 7 mm diameter wells were drilled into the agar. After that, the wells were filled with M6-QE at a concentration of 5 mg/mL. After 24–48 h of incubation at 28 °C, plates were examined. QSI activity was indicated by yellowish opaque bacterial growth around wells.[28] All tests were performed in triplicate.

Results and discussion

Torsion angles

Before the optimization process of the title molecule, the most stable conformer structure was determined to obtain the most accurate computer calculations.[29,30] In order to find the most stable structure, the torsional angles of the C–O bond between the quinoline ring and the methoxy group were changed and the minimum energy of the molecule was determined depending on the angles. The torsion angle between the quinoline ring and the methoxy group was fixed at 360° and was changed from 0° to 360° in 10° steps. At the end of this process, the minimum energy for the structure was found to be −324164.3 kcal/mol at 180°. The results were presented at Fig. 1. The optimization process for the title molecule was carried out on the structure that has minimum energy and the other calculations such as vibrational, thermodynamic, electronic, and nonlinear optical properties were also performed from the optimized structure.

Molecular structure

The optimized molecular structure of M6-QE is given in Fig. 2. The bond length and bond angle values of the structure are presented in Table 1. Also, X-ray data of M6-QE N-oxide dihydrate[31] are given in Table 1 and then this structure was compared with the title molecule. Root mean square deviation (RMSD) values were calculated

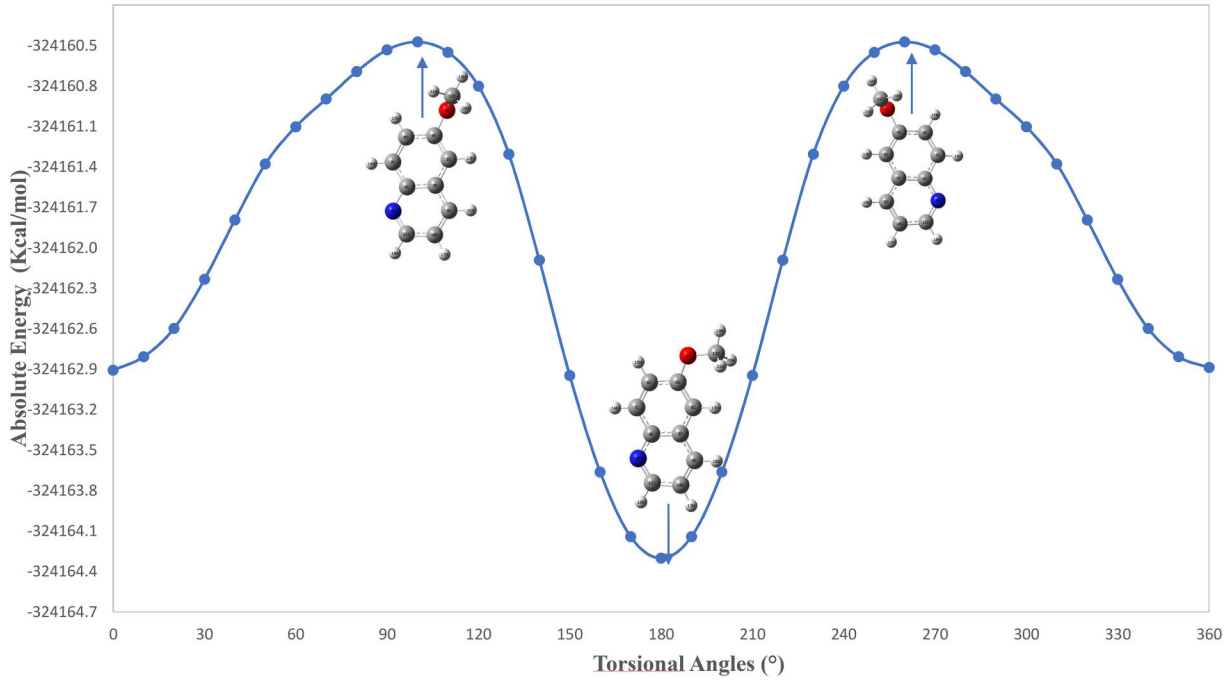

Figure 1. The torsional angle-energy graph of methyl 6-quinolyl ether.

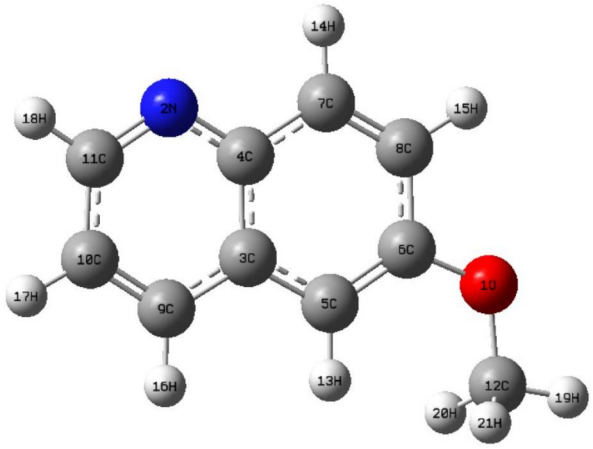

Figure 2. Optimized geometric structure of the M6-QE.

to compare the bond lengths and bond angles of these two structures. This value was found to be 0.083 for the bond lengths and 1.9066 for the bond angles.

The bond lengths of all C–C bonds for M6-QE were found to be between 1.428 and 1.367 Å in the theoretical calculations. These bond length values for M6-QE N-oxide dehydrate were given between 1.429 and 1.368 Å. The highest C–C bond length was found between C_3 and C_4 atoms from theoretical calculations, while the shortest value was found between C_7 and C_8 atoms. The highest and lowest values for XRD data were found at C_3–C_9 and C_9–C_{10} bonds, respectively.

Table 1. Optimized geometrical parameters of M6-QE.

	Bond lengths (Å)			Bond angles (°)	
Parameters	Calc.	XRD*	Parameters	Calc.	XRD*
O_1-C_6	1.362	1.372	C_6-O_1-C_{12}	118.41	116.89
O_1-C_{12}	1.422	1.434	C_4-N_2-C_{11}	117.99	122.26
N_2-C_4	1.361	1.401	C_4-C_3-C_5	119.97	118.37
N_2-C_{11}	1.317	1.343	C_4-C_3-C_9	117.09	118.73
C_3-C_4	1.428	1.415	C_5-C_3-C_9	122.94	122.90
C_3-C_5	1.421	1.426	N_2-C_4-C_3	122.82	118.34
C_3-C_9	1.416	1.429	N_2-C_4-C_7	118.76	121.08
C_4-C_7	1.422	1.420	C_3-C_4-C_7	118.42	120.58
C_5-C_6	1.378	1.382	C_3-C_5-C_6	119.83	120.43
C_5-H_{13}	1.082	0.950	C_3-C_5-H_{13}	118.58	119.80
C_6-C_8	1.422	1.418	C_6-C_5-H_{13}	121.59	119.80
C_7-C_8	1.367	1.371	O_1-C_6-C_5	125.15	126.11
C_7-H_{14}	1.083	0.950	O_1-C_6-C_8	114.51	113.72
C_8-H_{15}	1.084	0.950	C_5-C_6-C_8	120.34	120.15
C_9-C_{10}	1.374	1.368	C_4-C_7-C_8	120.81	119.61
C_9-H_{16}	1.085	0.950	C_4-C_7-H_{14}	117.83	120.20
C_{10}-C_{11}	1.414	1.400	C_7-C_8-H_{14}	121.36	120.20
C_{10}-H_{17}	1.084	0.950	C_6-C_8-C_7	120.62	120.82
C_{11}-H_{18}	1.087	0.950	C_6-C_8-H_{15}	117.87	119.60
C_{12}-H_{19}	1.089	0.980	C_7-C_8-H_{15}	121.50	119.60
C_{12}-H_{20}	1.095	0.980	C_3-C_9-C_{10}	119.42	120.06
C_{12}-H_{21}	1.095	0.980	C_3-C_9-H_{16}	119.62	120.00
RMSD	0.083		C_{10}-C_9-H_{16}	120.97	120.00
			C_9-C_{10}-C_{11}	118.93	120.39
			C_9-C_{10}-H_{17}	121.29	119.80
			C_{11}-C_{10}-H_{17}	119.82	119.80
			N_2-C_{11}-C_{10}	123.79	120.20
			N_2-C_{11}-H_{18}	116.45	119.90
			C_{10}-C_{11}-H_{18}	119.76	119.90
			O_1-C_{12}-H_{19}	105.91	109.50
			O_1-C_{12}-H_{20}	111.25	109.50
			O_1-C_{12}-H_{21}	111.25	109.50
			H_{19}-C_{12}-H_{20}	109.43	109.50
			H_{19}-C_{12}-H_{21}	109.43	109.50
			H_{20}-C_{12}-H_{21}	109.48	109.50
			RMSD	1.9066	

*Taken from Ref. [31].
(Å): Angstrom, (°): degree

The reason for these small differences in bond lengths is that the structures aren't exactly the same. That is, the XRD data belongs to the dehydrated structure of M6-QE. The molecule has two C–N bonds, and these bond lengths were found to be 1.361 (N_2-C_4) and 1.317 (N_2-C_{11}). The C–N bonds of M6-QE N-oxide dehydrate have different values. Since the O atom is attached to the N atom in this structure, we say that these values were determined differently for both structures. The O_1-C_6 and O_1-C_{12} bond lengths of the molecule used in our study were found to be 1.362 and 1.422 Å, respectively. The equivalent of these values in XRD data is 1.372 and 1.434 Å. The C–H bonds were obtained for M6-QE at values between 1.095 and 1.089 Å. According to the XRD data in the table, the bond length of six C–H bonds of M6-QE N-oxide dihydrate was 0.950 Å and the bond length of three of them was 0.980 Å. According to the XRD data of M6-QE N-oxide dihydrate, while six C–H bond lengths were found to be 0.950 Å, the other C–H bond lengths were determined to be 0.980 Å. M6-QE N-oxide dihydrate has two H_2O molecules in its crystal structure, and the bonding of the O atom to the nitrogen atom creates differences between the bond lengths. As can be seen from Table 1, the bond angle values calculated for the title molecule and the XRD values of the other structure are very close to each other. Small deviations were observed between the C–C–H, C–N–C, and N–C–H bond angles.[31]

Vibrational analysis

The vibrational spectrum is considered to be a unique physical property and is a characteristic of the molecule. The M6-QE molecule consists of 21 atoms, which have 57 modes of vibration. The calculated vibrational wavenumbers of 6-MQ for the B3LYP functional and 6–311++G (d.p) basis set have been given in Table 2, together with experimental values. The experimental and theoretical FT-IR and FT-Raman spectra of M6-QE molecule are given in Figs. 3 and 4.

While C–H stretching vibrations for aromatic molecules are defined in the range of 3100–3000 cm^{-1},[32,33] C–H stretching vibrations for methyl and methylene groups are defined in the range of 3000–2800 cm^{-1}.[34,35] In addition, in-plane and out-of-plane C–H bending vibrations are observed in the range of 1000–1300 and 750–1000 cm^{-1}, respectively.[36] In this study, the symmetrical C–H stretching vibrations in the benzene ring of the M6-QE molecule were calculated at 3057 cm^{-1} in theoretical calculations, while the asymmetrical C–H stretching vibrations were found at 3050 and 3042 cm^{-1}. Symmetrical C–H stretching vibrations for the pyridine ring were calculated at 3044 cm^{-1}, and asymmetrical C–H stretching vibrations at 3018 and 2988 cm^{-1}. In contrast to the theoretical asymmetric C–H stretching vibration calculated at 2988 cm^{-1}, a rather weak vibration mode was observed at 3025 cm^{-1} in the FT-IR spectrum and at 3003 cm^{-1} in the Raman spectrum. In-plane C–C–H bending modes of benzene and pyridine rings 1528, 1467, 1459, 1393, 1383.1359 cm^{-1}, 1279.1258 cm^{-1} is calculated at 1252, 1214, 1182, 1155, and 1132 cm^{-1}. The values corresponding to these bending modes are 1572, 1432, 1377, 1322, 1261, 1225, 1195, and 1160 cm^{-1} in the FT-IR spectrum and 1183 cm^{-1}. While the out-of-plane C–C–H bending vibrations of benzene and pyridine rings were calculated at 976, 852, 843, 790, 777, and 653 cm^{-1}, these vibration modes were experimentally determined. It was also observed in the FT-IR spectrum at 830 and 788 cm^{-1}.

While the symmetrical C–H stretching vibration for the methyl group was calculated at 2870 cm^{-1}, this vibration was observed at 2834 cm^{-1} in the FT-IR spectrum. Asymmetric C–H stretching vibrations for the methyl group are calculated at 2995 and 2927 cm^{-1}, while the corresponding experimental values are 3001 and 2934 cm^{-1}. The methyl group also includes symmetrical and asymmetrical bending vibrations according to the in-plane and out-of-plane bending of C–H bonds.[37] Symmetrical bending vibrations were calculated at 1467 and 1459 cm^{-1}. The FT-IR value for symmetrical bending vibration was measured at 1432 cm^{-1}. Asymmetric bending vibrations are calculated at 1502, 1497, and 1487 cm^{-1}, while the corresponding experimental FT-IR values are 1498 and 1472 cm^{-1}. In addition, in-plane rocking vibrations [34]

Table 2. Detailed vibrational assignments of M6-QE with total energy distribution.

		Theoretical				Experimental		
Mod	Sym	Freq	Freq*	I_{IR}	I_{RA}	FT-IR	FT-Ra	TED %
57	A′	3201	3057	3.1	23.5	–	3164 vw	82 υ_{CH}
56	A′	3194	3050	6.1	9.2	–	–	77 υ_{CH}
55	A′	3188	3044	11.8	29.9	–	3066 vw	82 υ_{CH}
54	A′	3185	3042	1.0	7.1	–	–	79 υ_{CH}
53	A′	3160	3018	5.9	8.8	–	–	79 υ_{CH}
52	A′	3139	2998	12.6	21.4	3025 vw	3003 vw	78 υ_{CH}
51	A′	3136	2995	14.4	18.1	3001 vw	–	81 υ_{CH}
50	A″	3065	2927	22.5	7.0	2934 vw	–	81 υ_{CH}
49	A′	3006	2870	29.9	24.2	2834 vw	–	91 υ_{CH}
48	A′	1659	1654	59.0	18.7	1621s	1659 w	30 υ_{CC} + 16 δ_{CCC} + 34 δ_{CCH}
47	A′	1633	1628	21.3	6.2	1595s	–	10 υ_{NC} + 23 υ_{CC} + 15 δ_{CCC} + 36 δ_{CCH}
46	A′	1604	1599	3.4	13.4	–	1631 vw	31 υ_{CC} + 15 δ_{CCC} + 26 δ_{CCH}
45	A′	1533	1528	53.1	1.9	1572 vw	1603 vw	21 υ_{CC} + 11 δ_{CCC} + 40 δ_{CCH}
44	A′	1506	1502	37.5	13.9	1498 vs	1505 w	11 υ_{CC} + 25 δ_{CCH} + 25 δ_{HCH} + 12 Γ_{COCH}
43	A′	1502	1497	0.8	11.2	–	1491 vw	14 υ_{CC} + 26 δ_{CCH} + 10 δ_{OCH} + 20 δ_{HCH} + 12 Γ_{COCH}
42	A″	1492	1487	6.2	9.8	1472 m	–	10 δ_{OCH} + 48 δ_{HCH} + 35 Γ_{COCH}
41	A′	1471	1467	0.8	8.3	–	–	11 υ_{CC} + 24 δ_{CCH} + 17 δ_{OCH} + 17 δ_{HCH}
40	A′	1463	1459	23.3	82.3	1432 m	1463 vs	15 υ_{CC} + 34 δ_{CCH} + 12 δ_{OCH} + 12 δ_{HCH}
39	A′	1397	1393	27.8	100.0	1377s	1400 vs	32 υ_{CC} + 28 δ_{CCH}
38	A′	1387	1383	9.4	5.5	–	–	15 υ_{CC} + 13 δ_{CCC} + 42 δ_{CCH}
37	A′	1363	1359	10.6	52.8	1322s	1365s	13 υ_{NC} + 25 υ_{CC} + 33 δ_{CCH}
36	A′	1283	1279	40.0	0.8	1261s	–	11 υ_{CC} + 14 δ_{CCC} + 46 δ_{CCH}
35	A′	1262	1258	1.3	0.6			18 δ_{CCC} + 43 δ_{CCH}
34	A′	1256	1252	100.0	2.9	1225 vs	–	10 υ_{OC} + 20 υ_{CC} + 10 δ_{CCC} + 24 δ_{CCH}
33	A′	1218	1214	14.0	3.0	1195 w	–	11 υ_{CC} + 22 δ_{CCH} + 24 δ_{OCH} + 10 δ_{HCH} + 14 Γ_{COCH}
32	A′	1186	1182	27.5	5.4	1160s	–	17 υ_{CC} + 35 δ_{CCH} + 13 δ_{OCH}
31	A″	1168	1165	0.4	2.6	–	–	41 δ_{OCH} + 12 δ_{HCH} + 11 Γ_{COCC} + 28 Γ_{COCH}
30	A′	1159	1155	0.0	2.3	–	–	15υ_{CC} + 68 δ_{CCH}
29	A′	1136	1132	16.0	7.1	1113s	–	13υ_{CC} + 15 δ_{CCC} + 50 δ_{CCH}
28	A′	1057	1053	22.8	18.9	1035s, sp	1057 w	11 υ_{OC} + 23υ_{CC} + 11 δ_{CCC} + 33 δ_{CCH}
27	A′	1050	1047	11.1	13.1	1023s	–	13υ_{OC} + 24υ_{CC} + 31 δ_{CCH}
26	A″	984	981	0.8	0.1	–	–	11 Γ_{CCCC} + 36 Γ_{CCCH} + 10 Γ_{NCCH} + 28 Γ_{HCCH}
25	A″	979	976	0.0	0.9	–	–	35 Γ_{CCCH} + 10 Γ_{NCCH} + 29 Γ_{HCCH}
24	A′	967	964	3.1	3.1	951 w	–	16υ_{CC} + 28 δ_{CCC} + 25 δ_{CCH}
23	A″	950	947	0.0	0.3	908 w	–	11 Γ_{CNCH} + 42 Γ_{CCCH} + 21 Γ_{HCCH}
22	A′	923	920	6.9	2.6	891 vw	–	16 υ_{CC} + 22 δ_{CCH} + 21 δ_{CCC}
21	A″	854	852	54.4	0.8	830 vs	–	13 Γ_{CCCC} + 44 Γ_{CCCH} + 15 Γ_{HCCO}
20	A″	845	843	0.2	0.6	–	–	19 Γ_{CCCC} + 43 Γ_{CCCH} + 11 Γ_{HCCO}
19	A″	792	790	7.5	0.3	788 s	–	13 Γ_{CCCC} + 50 Γ_{CCCH}
18	A′	783	780	2.3	85.5	768 s	784 vs	32 υ_{CC} + 21 δ_{CCH} + 22 δ_{CCC}
17	A″	779	777	1.6	0.2	–	–	27 Γ_{CCCC} + 34 Γ_{CCCH} + 10 Γ_{CCCN}
16	A′	723	720	6.6	8.7	709 s	721 vw	12 υ_{CC} + 22 δ_{CCH} + 29 δ_{CCC}
15	A″	655	653	0.2	0.2	–	–	29 Γ_{CCCC} + 31 Γ_{CCCH}
14	A′	632	630	5.2	1.4	616 s	–	10 υ_{CC} + 28 δ_{CCH} + 36 δ_{CCC}
13	A′	548	546	0.4	24.4	577 vw	546 w	14 υ_{CC} + 16 δ_{CCH} + 10 δ_{OCC} + 16 δ_{NCC} + 22 δ_{CCC}
12	A″	546	545	1.1	2.0	566 vw	–	22 Γ_{CCCC} + 23 Γ_{CCCH} + 11 Γ_{CCCN}
11	A′	513	512	1.1	13.6	–	511 vw	18 δ_{CCH} + 32 δ_{CCC} + 10 δ_{COC}
10	A″	480	479	3.5	0.3	–	–	32 Γ_{CCCC} + 36 Γ_{CCCH}
9	A′	442	441	4.3	40.5	–	441 m	14 υ_{CC} + 21 δ_{CCH} + 35 δ_{CCC}
8	A″	411	410	0.6	10.5	–	434 vw	34 Γ_{CCCC} + 26 Γ_{CCCH} + 10 Γ_{CCCN}
7	A′	354	353	3.1	15.1	–	357 vw	10 υ_{CC} + 14 δ_{CCH} + 12 δ_{NCC} + 35 δ_{CCC}
6	A″	316	315	1.9	0.3	–	–	21 Γ_{CCCC} + 20 Γ_{COCH} + 10 Γ_{NCCC} + 10 Γ_{CCCO}
5	A″	233	232	0.1	3.0	–	–	12 Γ_{CCCC} + 52 Γ_{COCH}
4	A′	199	198	0.6	49.7	–	196 m	15 υ_{CC} + 20 δ_{CCC} + 10 δ_{CCH} + 10 δ_{NCC} + 11 δ_{COC} + 22 δ_{OCC}
3	A″	178	178	3.7	1.3	–	–	29 Γ_{CCCC} + 20 Γ_{CCCH} + 11 Γ_{NCCC} + 10 Γ_{CCCO}
2	A″	135	135	0.4	42.0	–	133 m	27 Γ_{CCCC} + 12 Γ_{CCCH} + 18 Γ_{CCOC}
1	A″	80	80	0.7	96.9	–	91 vs	15 Γ_{CCCC} + 21 Γ_{COCH} + 11 Γ_{HCCC} + 26 Γ_{COCC}

vs: very strong, s: strong, m: medium, w: weak, vw: very weak
υ: stretching, δ: in-plane bending, Γ: torsion
For I_{IR}.and I_{Ra} relative intensity values normalized with highest peak absorption equal to 100.
*A scaling factors of 0.997 was used for frequencies with wavenumbers less than 1800 cm^{-1} and 0.955 for frequencies over than 1800 cm^{-1}.[19,20]

occurring in the methyl group were determined as 1165 cm^{-1} in the theoretical calculations for the M6-QE molecule, while the out-of-plane swing vibration was calculated at 1214 and 1182 cm^{-1}. In the experimental FT-IR spectrum, out-of-plane shaking vibrations were also observed at 1195 and 1160 cm^{-1}.

C–C and C=C stretching vibrations in aromatic molecule rings are observed in the range of 1650–1200 cm^{-1}.[37] The C=C stretching

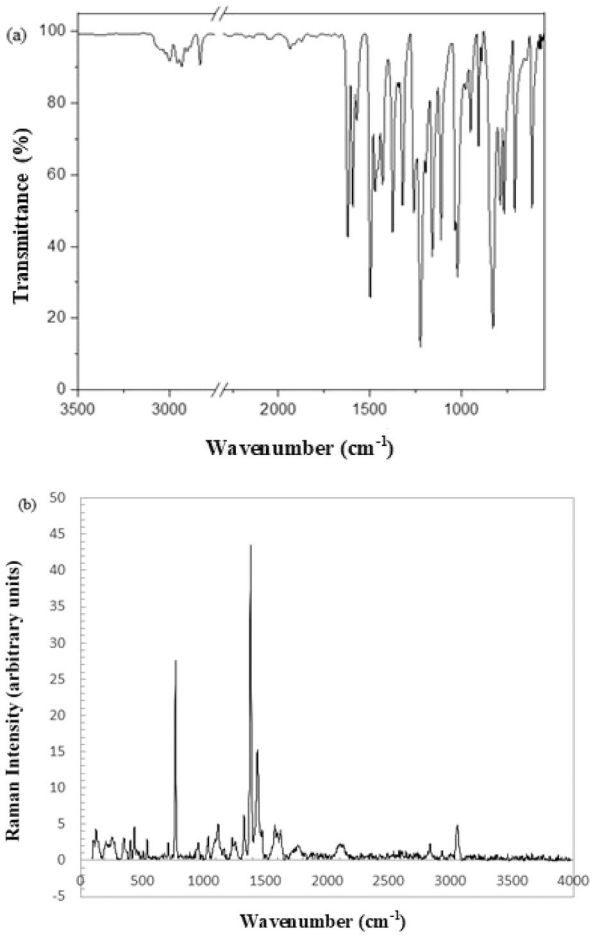

Figure 3. Experimental Fourier Transform (a) Infrared and (b) Raman spectra of M6-QE.

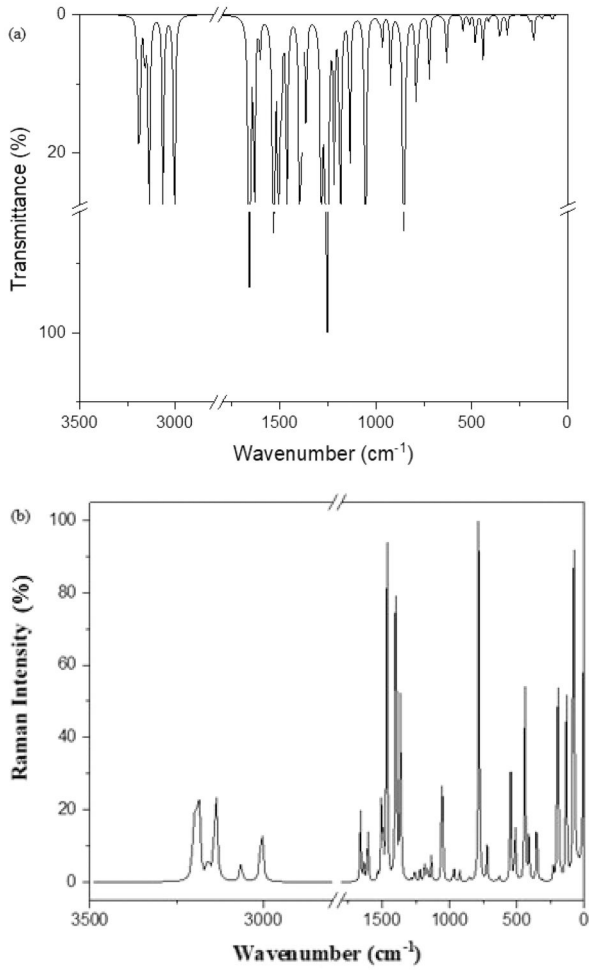

Figure 4. Theoretical Fourier Transform (a) Infrared and (b) Raman spectra of M6-QE.

vibration in the benzene ring of the M6-QE molecule was calculated at 1654 cm^{-1}, and the C=C stretching vibration in the pyridine ring at 1628 cm^{-1}. Experimental values corresponding to these theoretical values are 1621 and 1595 cm^{-1}. CC vibrations for the M6-QE molecule are 1595, 1528, 1502, 1497, 1467, 1459, 1393, 1383, and 1359 cm^{-1}, as a result of theoretical calculations. cm^{-1}, 1279, 1252, 1214, 1182, and 1155 cm^{-1} were found. These vibration modes were observed in the FT-IR spectrum at 1572, 1498, 1432, 1377, 1322, 1225, 1195, and 1160 cm^{-1}.

C–N stretching vibrations are generally observed in the range of $1342 - 266\ cm^{-1}$.[38] While these vibration values for the molecule were calculated at 1628 [1] and 1359 cm^{-1}, they were observed at 1595 and 1322 cm^{-1} in the FT-IR spectrum. On the other hand, 1365 cm^{-1} was observed in the FT-Raman spectrum. In addition, the O–C stretching vibrations for the M6-QE molecule were obtained from the theoretical calculations at 1252, 1053, and 1047 cm^{-1}, respectively, while the experimental FT-IR values were 1225, 1035, and 1023 cm^{-1}.

Frontier molecular orbital (HOMO and LUMO) analysis

In quantum chemical computing methods, it is very important to determine the energies of the HOMO and LUMO of a molecule. The determination of the energy values of these molecular orbitals is very important for the discovery of new materials, predicting optoelectronic properties, or filtering databases of organic molecules.[39] The HOMO and LUMO energies of M6-QE were calculated at the B3LYP/6–31++G(d,p) level of theory.

Table 3. HOMO, LUMO energies, and global reactivity descriptors of M6-QE.

No	Molecular orbital	Energy (eV)		Energy gap (eV)	Ionization potential (I) (eV)	Electron affinity (A) (eV)	Global hardness (η) (eV)	Electronegativity (χ) (eV)	Chemical potential (μ_c) (eV)	Global softness (σ) $(eV)^{-1}$	Global electrophilicity (ω) (eV)
1	H	−6.26	ΔE_{H-L}	4.61	6.26	1.65	2.30	3.96	−3.96	0.43	3.40
	L	−1.65									
2	H-1	−6.84	$\Delta E_{H_{-1}-L_{+1}}$	6.18	6.84	0.66	3.09	3.75	−3.75	0.32	2.28
	L + 1	−0.66									
3	H-2	−7.13	$\Delta E_{H_{-2}-L_{+2}}$	6.75	7.13	0.38	3.37	3.76	−3.76	0.30	2.09
	L + 2	−0.38									

H: HOMO (highest occupied molecular orbital); L: LUMO (lowest unoccupied molecular orbital); eV: electron volt; $(eV)^{-1}$: 1/electron volt.

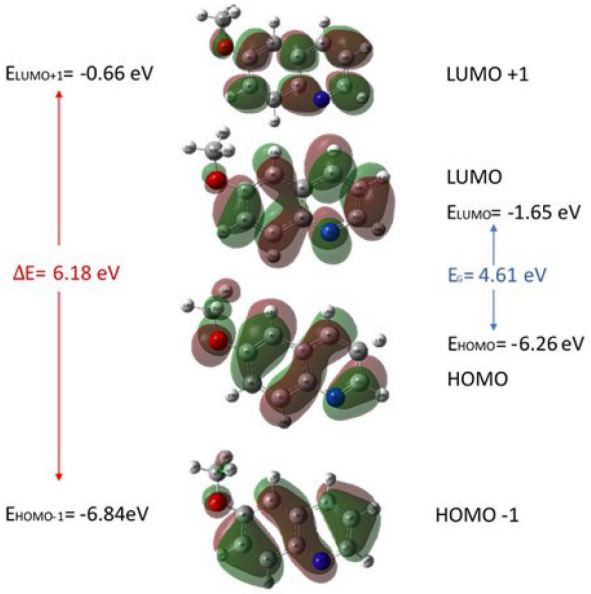

Figure 5. HOMO–LUMO diagrams of the M6-QE.

Also, determining the energy values of HOMO and LUMO of the molecule is very important in understanding the quantum chemical properties such as chemical hardness, chemical potential, reactivity, kinetic stability, chemical softness, electronegativity, electrophilicity, and optical polarizability. All these properties of the title molecule are given in Table 3. HOMO–LUMO energies of the orbitals and some quantum chemical properties of the M6-QE were calculated according to the following equations: $I = -E_{HOMO}$, $A = -E_{LUMO}$, $\eta = (-E_{HOMO} + E_{LUMO})/2$, $\mu_c = (E_{HOMO} + E_{LUMO})/2$, $\chi = -\mu_c$ and $\omega = \mu_c^2/2\eta$.[35] As seen from Fig. 5, HOMO and LUMO levels are spread over the entire molecule, except for the methyl group in the ground and first excited states. The HOMO–LUMO gap value of M6-QE is equal to 4.61 eV. This value is relatively high. Therefore, we can say that the title compound has high chemical stability and low reactivity.[40] Chemical hardness (η); ionization potential (I), and electron affinity (A) for the title molecule are calculated to be 2.30, 6.26, and 1.65 eV, respectively. The calculated electrophilicity (ω) value is 3.40 eV. Since this parameter is higher than 1.5 eV, the molecule has a strong structure.[36]

Molecular electrostatic surface map (MEP)

The MEP surface map provides visual information about a molecule's electrophilic and nucleophilic regions and hydrogen bond interactions. In addition, information about charge distributions is obtained. It helps explain how atoms interact with each other and, as a result, the nature of chemical bonds. Of the colored regions on this map, the red-colored areas represent electron-rich regions, while the blue-colored regions represent electron-poor regions, that is, positive regions. The green-colored regions represent the zero potential region. Other intermediate colors are at a medium level, and the electrostatic potential color order from negative regions to positive regions is as follows: red (orange) yellow < green < blue.[41,42]

The MEP surface map of the M6-QE molecule is given in Fig. 6. According to this map, the atoms in the most electronegative region are N in the red region and O in the orange region, respectively. Since almost all the C atoms in the aromatic rings are located in the yellow region, it was determined that these atoms are slightly electron rich. Since the hydrogen atoms in both the aromatic rings and the OCH3 carboxyl group are in the blue-colored region, these groups are electron weak and are in the positive region. In addition, a two-dimensional contour map showing MEP surface values is given in Fig. 7. As seen from this map, the entire molecule is located in

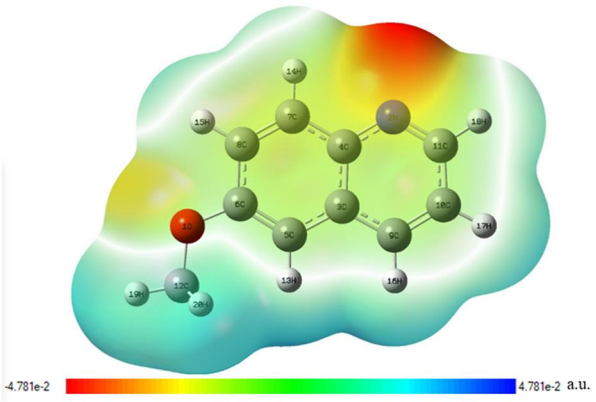

Figure 6. The molecular electrostatic potential 3D map of M6-QE (all in arbitrary unit).

the region of less negative potential, which is colored yellow.

Thermodynamic properties

Thermodynamic functions were calculated based on vibration analysis using the 6–311++ G (d,p) basis set in the gas phase. Entropy (S), enthalpy changes (ΔH), Gibbs free energies (G), and heat capacities (Cp) of M6-QE at constant pressure and different temperatures (100–1000 K) were calculated. Thermodynamic parameters obtained from theoretical calculations are listed in Table 4. In Fig. 8, thermodynamic parameter graphs are presented depending on the temperature. Thermo-molecular properties such as base vibration energy, enthalpy, Gibbs free energy, entropy, heat capacity, and thermal energy are important in material characterization.[43] Since it is a characteristic property of molecules, the base point vibrational energy is constant at all temperatures. The ground vibration energy obtained as a result of the optimization of the M6-QE molecule was calculated as −324164.3 kcal/mol. While all the thermodynamic parameters showed an increase due to the increase in molecular vibrations depending on the increasing temperature, G was calculated to decrease with the increase in temperature (Fig. 8). Entropy and enthalpy changes indicate that the molecule has the flexibility to change its thermodynamic system with temperature increase. The thermodynamic properties calculated in this study reveal important and useful information for future studies on M6-EQ.

Fukui functions

According to the Fukui frontier molecular orbital theory, the chemical reactivity of a molecule is interpreted in terms of the molecule's HOMO or LUMO electron density. The electrophilic and nucleophilic nature of each atom in the molecule is calculated using Fukui functions based on population analysis. Fukui functions are also known as the method of adding or removing an electron from the molecule. Fukui function charges are obtained using Mulliken population analysis. Fukui functions are calculated with the following equations.[44–47]

$$f_k^- = q_k(N) - q_k(N-1) \tag{7}$$

Electrophilic attack

$$f_k^+ = q_k(N+1) - q_k(N) \tag{8}$$

Nucleophilic attack

$$f_k^0 = \frac{1}{2}\left[q_k(N+1) - q_k(N-1)\right] \tag{9}$$

Neutral attack

In these equations, q_k is the rth. is the atomic charge in the region, and the numbers n, n + 1, and n-1 are the total number of electrons in the neutral, anion, and cation states. The highest value of $f^+(r)/f^-(r)$ represents relative electrophilicity, while the highest value of $f^-(r)/f^+(r)$ represents relative nucleophilicity.[47,48] Information on Fukui functions is given in Table 5. According to the $f^+(r)/f^-(r)$ ratio, the electrophilic atoms of the molecule during any reaction were determined as O_1, C_3, C_4, C_5, C_6, C_{12}, H_{13}, H_{19}, H_{20}, and H_{21}. According to the $f^-(r)/f^+(r)$ ratio, the atoms of the molecule that show nucleophilic behavior during any reaction were determined as N_2, C_7, C_8, C_9, C_{10}, H_{14}, H_{15}, H_{16}, H_{17}, and H_{18}. Fukui function data obtained from $f^+(r)/f^-(r)$ and $f^-(r)/f^+(r)$ ratios compared with molecular electrostatic surface map O_1 atom and C_3, C_4, C_5, C_6 atoms while H16, H17, and H18 atoms were determined as electrophilic in both analysis methods, they were determined as nucleophilic in both methods. According to the Fukui functions, the N_2 atom exhibits nucleophilic behavior, while the N_2 atom is in the electrophilic region in the molecular electrostatic surface map.

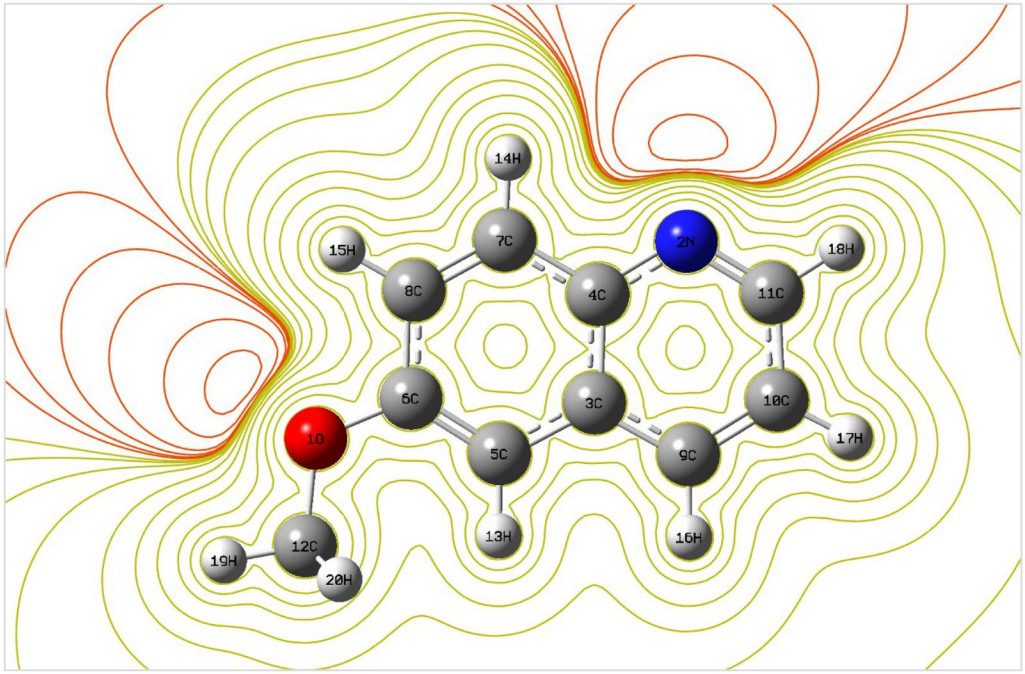

Figure 7. Two-dimensional contour map of molecular electrostatic potential surface for M6-QE.

Table 4. Thermodynamic properties at different temperatures of M6-QE.

T (K)	$C^0_{p,m}$ (J mol^{-1} K^{-1})	S^0_m (J mol^{-1} K^{-1})	ΔH^0_m (kJ mol^{-1})	G_{corr} (kJ mol^{-1})	ε_{ZPE} (kJ mol^{-1})
100	281.71	57.29	1.09	415.20	−1355864.85
200	341.21	104.39	3.21	384.00	−1355864.85
300	396.83	157.34	6.53	347.12	−1355864.85
400	451.65	208.71	11.11	304.71	−1355864.85
500	504.97	252.79	16.83	256.90	−1355864.85
600	555.87	288.72	23.51	203.87	−1355864.85
700	603.92	317.81	30.97	145.89	−1355864.85
800	649.08	341.62	39.05	83.26	−1355864.85
900	691.47	361.37	47.65	16.26	−1355864.85
1000	731.30	377.93	56.69	−54.85	−1355864.85

$C^0_{p,m}$: Heat capacity, S^0_m: Entropy , ΔH^0_m: Enthalpy changes, G_{corr}:Gibbs free energy, ε_{ZPE}: Zero-point energy.

In addition, a clear distinction is made between nucleophilic and electrophilic attack at a given region with the dual descriptor Δf(r) marks. The binary identifier from the Fukui functions is calculated with the following formula.

$$\Delta f(r) = f^+(r) - f^-(r)$$

When Δf(r)>0, that region is preferred for a nucleophilic attack, while when Δf(r)<0 that region is preferred for an electrophilic attack.[49,50] The highest positive values for the binary descriptor were determined as $O_1 > C_5 > C_6 > C_4$, respectively, and these atoms represent electrophilic regions. The largest negative binary identifier values were found as $C_8 > C_9 > C_{10} > N_2$, respectively, and these atoms also show nucleophilic regions.

Fukui function data obtained from $f^+(r)/f^-(r)$ and $f^-(r)/f^+(r)$ ratios and binary descriptors compared with molecular electrostatic surface map O_1 atom and C_3, C_4, C_5, C_6 atoms were determined as electrophilic in both analysis methods, while H16, H17 and H18 atoms were determined as nucleophilic in both methods. According to the Fukui functions, the N2 atom exhibits nucleophilic behavior, while the N_2 atom is in the electrophilic region in the molecular electrostatic surface map. It was concluded that the Fukui Functions agreed with the molecular electrostatic surface map analysis.

Nonlinear optical properties

In this study, the dipole moment, polarizability and first-order hyperpolarizability properties (μ, α, and β_0) of the M6-QE molecule were calculated using the DFT/B3LYP method with the

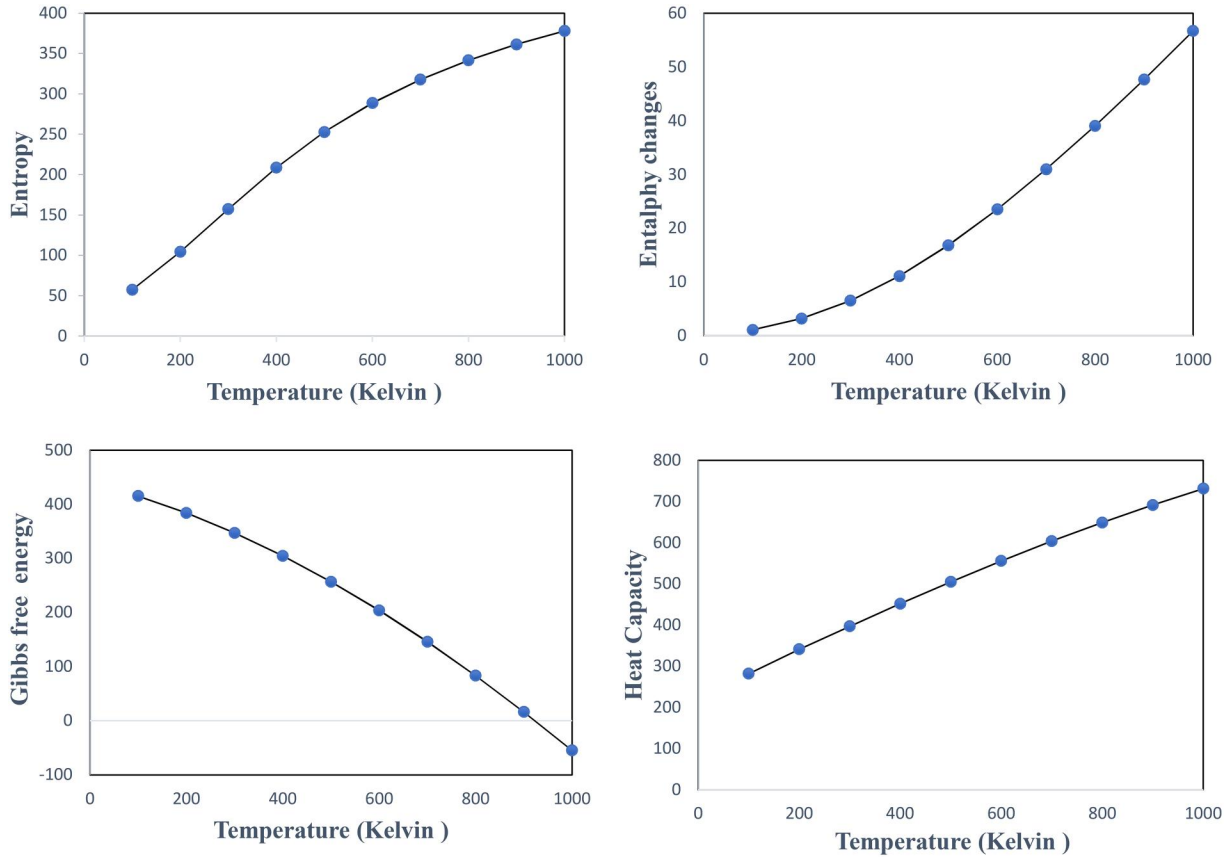

Figure 8. Temperature-dependent thermodynamic parameters of the 6-MQ molecule.

Table 5. Condensed Fukui functions calculated from Hirshfeld charges.

Atoms	f^+	f^-	f^0	f^+/f^-	f^-/f^+	$\Delta f(r)$
O_1	0.095	0.027	0.061	**3.557**	0.281	0.068
N_2	0.054	0.089	0.071	0.604	**1.657**	−0.035
C_3	0.026	0.020	0.023	**1.282**	0.780	0.006
C_4	0.049	0.027	0.038	**1.841**	0.543	0.022
C_5	0.103	0.054	0.078	**1.890**	0.529	0.048
C_6	0.076	0.046	0.061	**1.650**	0.606	0.030
C_7	0.065	0.075	0.070	0.871	**1.148**	−0.010
C_8	0.034	0.081	0.058	0.422	**2.368**	−0.047
C_9	0.056	0.098	0.077	0.576	**1.736**	−0.041
C_{10}	0.046	0.082	0.064	0.560	**1.786**	−0.036
C_{11}	0.083	0.078	0.080	1.069	0.935	0.005
C_{12}	0.026	0.016	0.021	**1.620**	0.617	0.010
H_{13}	0.038	0.029	0.033	**1.293**	0.774	0.008
H_{14}	0.037	0.042	0.039	0.879	**1.138**	−0.005
H_{15}	0.031	0.045	0.038	0.697	**1.435**	−0.014
H_{16}	0.030	0.048	0.039	0.626	**1.597**	−0.018
H_{17}	0.033	0.049	0.041	0.673	**1.485**	−0.016
H_{18}	0.041	0.048	0.044	0.845	**1.183**	−0.007
H_{19}	0.029	0.022	0.026	**1.335**	0.749	0.007
H_{20}	0.025	0.013	0.019	**1.866**	0.536	0.011
H_{21}	0.025	0.013	0.019	**1.866**	0.536	0.011

f^+: nucleophilic attack, f^-: electrophilic attack, f^0: neutral attack, Δf(r): dual descriptor.

6–311++G(d,p) basis set. Data of nonlinear optical properties are listed in Table 6.

In the presence of an applied electric field, the energy of a system is a function of the electric field. The first hyperpolarizability is a tensor that can be defined by the 3x3x3 matrix. The 27 components of the 3-dimensional matrix can be reduced to 10 components due to the Kleinman[51] symmetry.[52] The components of μ, α and β are defined as coefficients in the Taylor series expansion of energy in the external electric field. When the external electric field is weak and homogeneous, the energy is also weak and homogeneous and is given by the following equation.

$$E = E^0 - \mu_\alpha F_\alpha - \frac{1}{2}\alpha_{\alpha\beta}F_\alpha F_\beta - \frac{1}{6}\beta_{\alpha\beta\gamma}F_\alpha F_\beta F_\gamma + \ldots$$

Here E_0 is the energy of the unperturbed molecules, F_α is the electric field at the origin. μ is the dipole moment component. Alpha beta and gamma are the polarizability, first hyperpolarizability, and second hyperpolarizability tensors, respectively.

Total static dipole moment (μ), average polarizability (α) and initial hyperpolarizability (β_0) are given by the following equations using x, y, z components.

Table 6. The electric dipole moment μ (Debye), Polarizability α ($10^{-24}esu$) ve hyperpolarizebility β_0 ($10^{-30}esu$) of the title molecule.

Dipole moment		Polarizability			Hyperpolarizability		
μ_x	−0.01	α_{xx}	42.78	β_{xxx}	0.01	β_x	0.01
μ_y	13.56	α_{yx}	0.00	β_{xxy}	−0.70	β_y	1.82
μ_z	0.01	α_{yy}	36.43	β_{xyy}	0.00	β_z	0.35
μ	13.56	α_{zx}	−0.96	β_{yyy}	2.18	β_0	1.85
		α_{zy}	−0.01	β_{xxz}	0.00	β	0.00
		α_{zz}	15.44	β_{xyz}	0.35		
		$\bar{\alpha}$	31.55	β_{yyz}	0.00		
		$\Delta\alpha$	24.84	β_{xzz}	0.00		
				β_{yzz}	0.35		
				β_{zzz}	0.00		

$$\left|\overline{\alpha}\right| = \frac{1}{3}\left(\alpha_{xx} + \alpha_{yy} + \alpha_{zz}\right)$$

$$\Delta\alpha = \frac{1}{\sqrt{2}}\left[\left(\alpha_{xx} - \alpha_{yy}\right)^2 + \left(\alpha_{xx} - \alpha_{zz}\right)^2 + \left(\alpha_{yy} - \alpha_{zz}\right)^2 + 6\left(\alpha_{xy}^2 + \alpha_{xy}^2 + \alpha_{xy}^2\right)\right]^{1/2}$$

$$\beta_0 = \left[\left(\beta_{xxx} + \beta_{xyy} + \beta_{xzz}\right)^2 + \left(\beta_{yyy} + \beta_{xxy} + \beta_{yzz}\right)^2 + \left(\beta_{zzz} + \beta_{xxz} + \beta_{yyz}\right)^2\right]^{1/2}$$

$$\mu = \frac{1}{3}\left(\mu_x^2 + \mu_y^2 + \mu_x^2\right)$$

A large specific component of polarizability and hyperpolarizability indicates a delocalization of the charge. Polarizability values are given in atomic units (a.u.) in Gaussian 09 calculations. These values are converted to electrostatic unit (esu) using conversion factors such as ($\Delta\alpha$ (10–24 esu) and β_0 (10–30 esu)). The first hyperpolarizability (β_0) of the compound was calculated as 1.85×10–30 esu. This value is 5 times greater than the value of urea (urea $\beta_0 = 0.3728 \times 10$–30 esu) chosen as the reference molecule. Therefore, it was concluded that the M6-QE molecule can be used as a nonlinear (NLO) material.[30,53]

Charge analysis

The electronic charges of atoms determine the binding potential of a molecule and the reactivity of the molecules. Atomic charges also affect many properties of the molecule, such as molecular moment, molecular polarity, and electronic structure. In addition, atomic charges are used in the calculation of Fukui functions. Therefore, the determination of charge density values has an important place in quantum chemical calculations.[54–56]

Table 7. Comparison of NBO, Hirshfeld and APT atomic charges for M6-QE.

Atoms	APT	Hirshfeld	NBO
O_1	−0.959	−0.13979	−0.538
N_2	−0.310	−0.19201	−0.441
C_3	0.036	−0.00614	−0.076
C_4	0.053	0.048319	0.150
C_5	−0.225	−0.07912	−0.276
C_6	0.687	0.074668	0.327
C_7	0.057	−0.03633	−0.166
C_8	−0.124	−0.04941	−0.218
C_9	0.090	−0.03268	−0.151
C_{10}	−0.123	−0.05177	−0.242
C_{11}	0.142	0.024869	0.058
C_{12}	0.499	−0.00778	−0.205
H_{13}	0.045	0.042872	0.208
H_{14}	0.054	0.054445	0.219
H_{15}	0.058	0.05548	0.220
H_{16}	0.031	0.051803	0.203
H_{17}	0.035	0.051058	0.210
H_{18}	0.007	0.049104	0.183
H_{19}	0.003	0.055238	0.193
H_{20}	−0.028	0.043529	0.170
H_{21}	−0.028	0.043529	0.170

After the M6-QE molecule was optimized with the B3LYP/6–311++G(d, p) base set, the electron population of each atom was calculated for the same base set by natural bond orbital (NBO), Hirshfeld, and atomic polar tensor (APT) analyses. Calculated charge values are listed in Table 7 and presented in Fig. 9. For the three-charge analysis, O_1, N_2, C_5, C_8, and C_{10} atoms were found to be negatively charged, while C_4, C_6, C11, H_{13}, H_{14}, H_{15}, H_{16}, H_{17}, H_{18}, and H_{19} atoms were found to be positively charged. The data obtained from the charge analysis agrees with both the results obtained from the Fukui functions and the results obtained from the molecular electrostatic surface map.

In Table 7, negative values for all three charge methods are represented by the red regions in Fig. 9. The positive charges in the chart correspond to the blue region in the MEP map. When the data obtained from both the Fukui functions and the molecular electrostatic surface map are compared with the results obtained from the charge analysis, it is seen that the atoms and regions that behave as nucleophilic (positive) and electrophilic (negative) in all three methods are in harmony. Thanks to the information obtained from the Fukui functions, MEP map, and charge

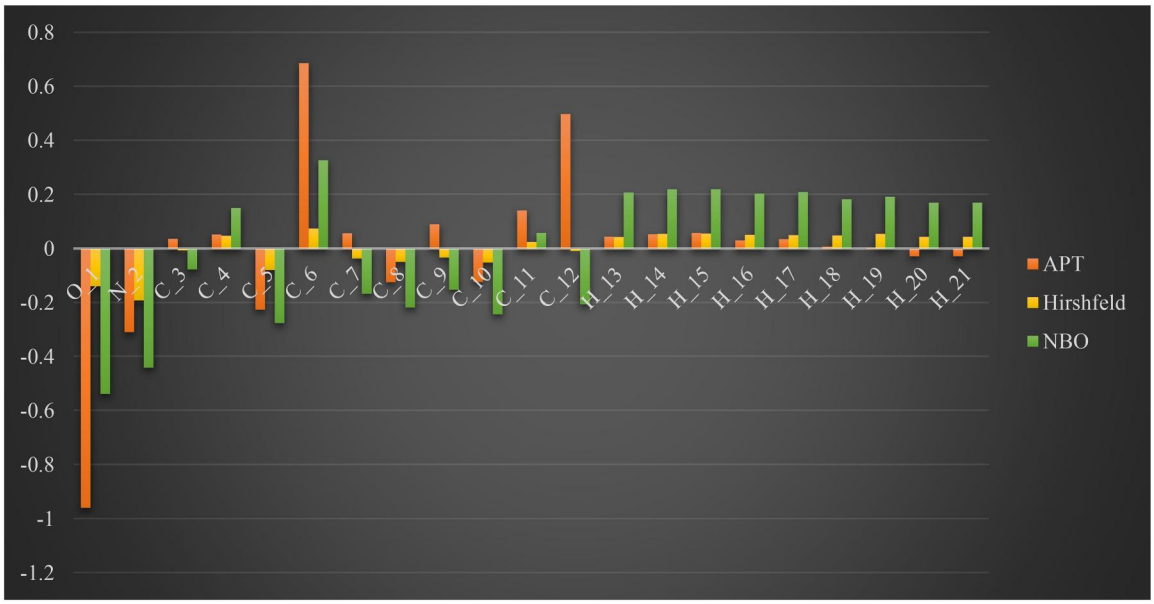

Figure 9. Natural bond orbital, Hirshfeld, and atomic polar tensor electron charge distribution for M6-QE.

analysis, it can be determined which atom or atoms will bond with a higher probability when the M6-QE molecule reacts.

Nuclear magnetic resonance (^{1}H and ^{13}C) analysis

Chemical shift analysis of nuclear magnetic resonance is one of the most widely used methods in the structural analysis of organic molecules.[55] While the ^{1}H NMR spectrum provides information about the existence of protons in the structure and their relationship with the C atoms to which they are attached, the ^{13}C spectrum determines the C atoms in the structure. Theoretical ^{1}H and ^{13}C NMR calculations of M6-QE were carried out in DMSO solvent in the DFT/B3LYP approach with the GIAO method by using the 6–311 + G(2d,p) basis set.

The theoretical chemical shift values of H atoms of M6-QE are as follows: (H13) 7.30, (H14) 7.63, (H15) 7.74, (H16) 8.32, (H17) 8.38, (H18) 9.06, (H19) 4.20, and (H20-H21) 3.88 ppm. The experimental data corresponded to theoretical values of 6.63, 6.96, 7.06, 7.60, 7.74, 8.46, 3.57, 3.47, and 3.41 ppm, respectively. The chemical shift values obtained for carbon atoms in ^{13}C NMR calculations are also as follows: (C3) 135.39, (C4) 151.45, (C5) 107.33, (C6) 165.70, (C7) 137.10, (C8) 127.49, (C9) 139.43, (C10) 125.29, (C11) 152.69, and (C12) 55.95 ppm. The signals in the experimental ^{13}C NMR spectrum corresponding to these values were observed at 129.51, 144.30, 106.10, 157.63, 130.82, 122.08, 135.20, 122.45, 148.34, and 58.90 ppm.

The correlation graphs between experimental and calculated ^{1}H and ^{13}C NMR values are presented in Fig. 10. According to the R^2 results, experimental and theoretical chemical shift values of ^{1}H and ^{13}C NMR for the M6-QE molecule are in good agreement with each other.

As a result, a complete structural analysis of the M6-QE molecule was performed by performing experimental and theoretical chemical shift analysis for both H atoms and C atoms, and the experimental spectra also support the geometry of M6-QE.

Electron localization function (ELF) and (localized orbital locator)LOL analysis

ELF and LOL analysis were performed with the Multiwfn program [21] in order to determine the molecular space regions where the probability of finding an electron is high. Both analyses are surface analyses based on covalent bonds, and localized and delocalized electron regions are determined. While ELF analyses are performed according to electron pair density, LOL analyses are performed according to the situation in which localized orbitals are maximized.[57,58] ELF and

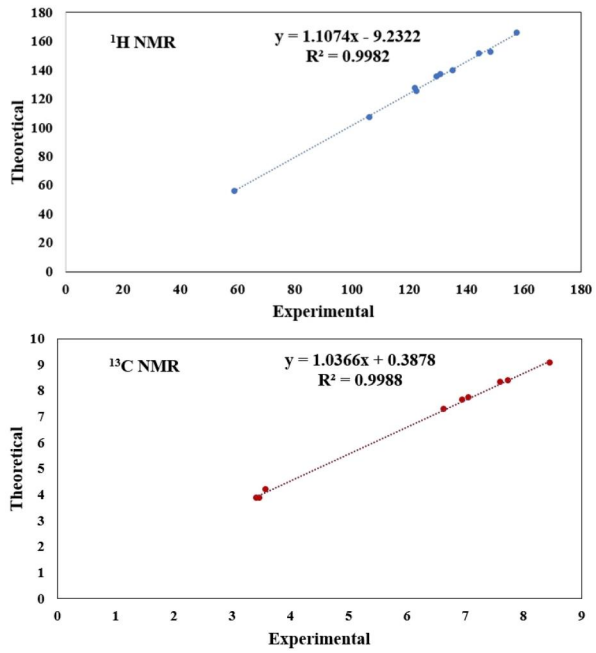

Figure 10. Correlation graphics between theoretical and experimental ^{1}H and ^{13}C NMR values of M6QE.

LOL maps of 6-MQ are given in Fig. 11a and b. Color-filled map and 3D surface shaded projection map of ELF.

The ELF value of the molecule ranges from 0.0 to 1.0 values between 0.5 and 1.0 indicate localized electron regions, while values less than 0.5 indicate delocalized electron regions. According to Fig. 11(a), there are localized electrons in the high ELF regions around all hydrogen atoms and between the atom bonds in the benzene and pyridine rings of M6-QE. In addition, high red LOL values are concentrated in the region between the C atoms of the title molecule, while the blue regions on the C atoms show the depletion regions between the valence and the inner shell. Finally, the white regions on the H atoms in the LOL map indicate that the electron density exceeds the upper scale value of 0.8.

Antimicrobial activity of M6-QE molecule on bacteria and yeast

Infectious diseases have become a global health threat due to the emergence and spread of resistant microorganisms. As a result, there is a constant need for new antimicrobial drugs and therapeutic techniques to be developed. Quinolines and quinolones have been isolated from plants, animals, and

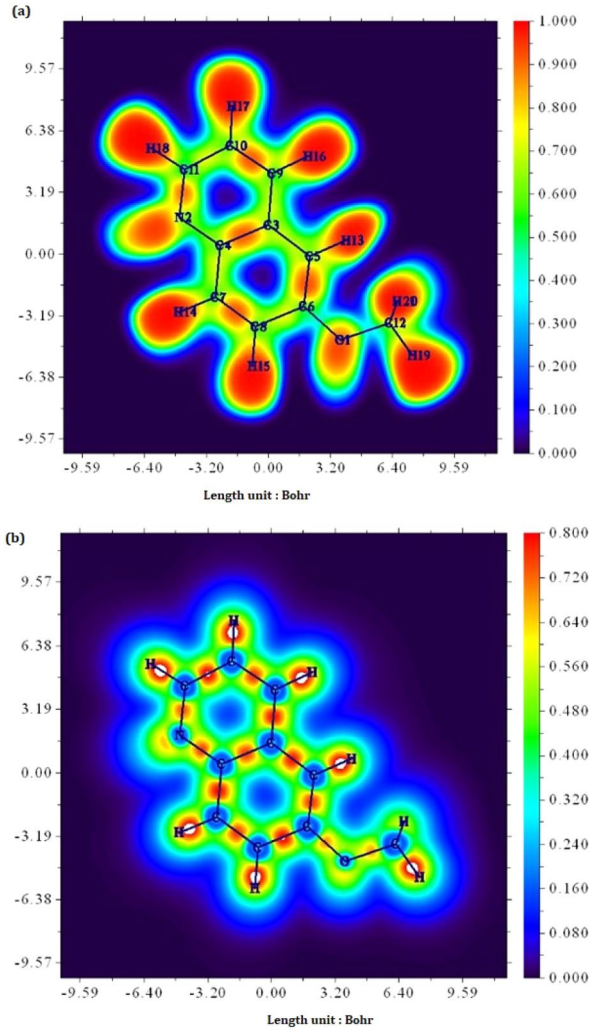

Figure 11. Relief map and color filled map of (a) ELF (b) LOL of M6-QE.

microbes and have exhibited antibacterial, insecticidal, anti-inflammatory, antiplatelet, and anticancer properties.[59]

Inhibition sites and MICs are summarized in Table 8. M6-QE showed antimicrobial activity against all tested microbial strains (inhibition zone diameters ranging from 15 to 30 mm) (Table 8). DMSO was used as a control that did not exhibit antimicrobial activity. All bacterial strains were found to be susceptible to M6-QE. The largest zones of inhibition were found for M6-QE against *K. pneumoniae* (22.4 mm) and against *B. subtilis* (19.8 mm). The antimicrobial activity of compound M6-QE was evaluated with reference strains, MIC tests, and agar well diffusion tests.

Table 8. Minimal inhibitory concentration (MIC) and the inhibition zone diameter (mm) of M6-QE against evaluated bacteria and yeast.

		MIC (μg/mL)						
Bacteria	DIZ (mm)	16	32	64	128	AMP (10μg)	Nystatin	DMSO 10%
E. coli ATCC 25922	12.4	–				16	–	–
P. aeruginosa ATCC 27853	15.8	–				18	–	–
*S.typhimurium*ATCC 14028	15.6	–				18	–	–
S. dysenteriae ATCC 11835	15.8	16				18	–	–
A.hydrophila ATCC 7966	13.2	16				–	–	–
K. pneumoniae ATCC13883	22.4		32			15	–	–
S.aureus ATCC25923	12.4	16				Na	–	–
B. cereus 709 Roma	13.4		32			16	–	–
B. subtilis ATCC 6633	19.8			64		15	–	–
C. albicans ATCC 90028	16.2				128	–	20	–
C. violeceum ATCC 12472 (Antiquorum-sensingactivities)	34.2	16				Nt	–	–

MIC (μg/mL): minimum inhibitory concentration; DIZ (mm): diameter of inhibition zone (mm)
Positive control: AMP (10 μg): ampicillin
Negative control: 10% DMSO
nt: not tested.
na: no activity (no inhibition zone detected).
Note: – indicates no inhibition
–: No antimicrobial activity was detected in agar well diffusion method and MIC

Results from the MIC test showed that M6-QE can inhibit the growth of gram-negative and gram-positive bacteria and yeast with MIC values of 16, 32, 64, and 128 μg/mL, respectively. M6-QE MIC results were greater than 16 μg/mL in all strains (Table 8). Compound M6-QE showed activity for *S. dysenteriae, A. hydrophila,* and *S. aureus* with a MIC value of 16 μg/mL. In addition, the compound showed activity for *K. pneumoniae* and *B. cereus* with an MIC value of 32 μg/mL. The same compound showed activity for *B. subtilis* and *C. albicans* with MIC values of 32 and 128 μg/mL, respectively, but not for *E. coli, P. aeruginosa,* and *S. typhimurium,* which did not show any effect.

Table 8 summarizes the inhibitory zones of compound M6-QE. The chemical exhibited antibacterial efficacy against all bacterial strains tested (zones of inhibition ranging from 15 to 30 mm in diameter).

As a control, DMSO was utilized, which had no antibacterial activity. M6-QE sensitivity was observed to be higher in all bacterial strains.

The largest inhibition zones were found against *K. pneumoniae* (22.4 mm) and *B. subtilis* (19.8 mm) for M6-QE. The antimicrobial activities of M6-QE (Table 8; DIZ values of 12.4–22.4 mm) were even better than those of ampicillin (DIZ values of 15–18 mm) against patogen bacteria. The same compound exhibited similar antifungal activity (DIZ values of 16.2 mm) as Nystatin (20 mm). The antimicrobial activity of M6-QE was compared with the standard reference antibiotics ampicillin and nystatin and it was concluded that it can be considered as an antimicrobial agent since it showed significant inhibition against some pathogenic bacteria.

The M6-QE has good potential to enable the use of disinfected medical and surgical instruments in clinical and surgical procedures that are important to patients. In particular, *K. pneumoniae* bacteria is a risky pathogen for patients and hospitals.

Antiquorum-sensing effect of M6-QE

In bacteria and fungi, QS is a cell-to-cell communication system that governs virulence factor production and biofilm formation.[60,61]

The antimicrobial efficacy of molecule M6-QE against pathogenic microorganisms has been impressive. A molecule is essential to the development of novel medications. There is presently no explanation for its pharmacokinetic properties, efficacy in the body, spectrum of action against clinical isolates, or potential toxicity to people. Of course, these results were achieved in vitro. The antimicrobial activity may be affected by the compound's concentration, the strain type being studied, and the temperature and humidity levels. Since antibiotics are used therapeutically, further research and in vivo studies are required.

Table 9. Molecular docking result of M6-QE molecule with proteins.

Molecule	Protein (PDB ID)	Binding energy (kcal/mol)	Inhibition Constant K_i (μM)	Reference RMSD (Å)
M6-QE	3D02	−7.14	5.88	23.01
	4OZ5	−5.23	146.46	39.92

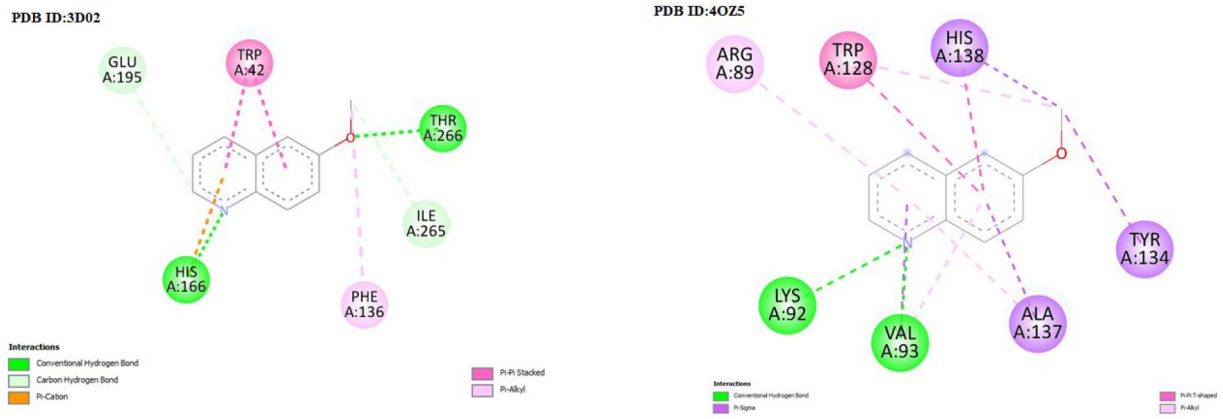

Figure 12. 2D visual representations of ligand and proteins.

Table 10. Protein–ligand interaction parameters with hydrophobic contacts for M6-QE molecule.

Molecule	Protein (PDB ID)	Hydrogen bonded amino acid residue	H-Bonded distance (Å)	Hydrophobic interacted amino acid residue
M6-QE	3D02	HIS A:166	2.17	TRP A:42
		THR A:266	2.00	
		LYS A:36	2.75	
	4OZ5	VAL A:93	2.11	ALA A:137
		LYS A: 92	2.34	TRP A:128
				HIS A:138

Molecular docking of M6-QE

The molecular docking study was carried out to support biological activity studies. The M6-QE molecule showed high activity on *K. pneumoniae* ATCC 13883 and *B. subtilis* ATCC 6633 microorganisms. For this reason, the protein structures of these two microorganisms (3D02 and 4OZ5) were selected from the PDB protein database,[24] the ligand–protein interactions were examined, and the dominant binding modes were predicted.[62] First of all, the M6-QE ligand and selected proteins of microorganisms were converted to pdbqt format to be used in molecular docking studies. Then, the water molecules in the proteins were deleted, and polar hydrogen atoms and Kollman charges were added. To define the active sites of proteins, a grid box with $40 \times 40 \times 40$ points and 0.375 Å grid spacing was created and centered on the selected proteins. Molecular docking studies were carried out with the AutoDockTools.[23] The obtained data is presented in Tables 9 and 10. Additionally, the images obtained using the Discovery Studio Visualizer package program are presented in Fig. 12.[25] The M6-QE molecule is docked to the reactive regions of the 3D02 and 4OZ5 proteins with binding energies of −7.14 and −5.23 kcal/mol, respectively. When predicting whether a molecule will function as a therapeutic candidate, one crucial statistic to consider is the inhibition constant, or Ki value. A medication molecule's Ki value shouldn't be greater than the range of 10 nanomolar.[63] The Ki value obtained for the 3D02 protein is 5.88 μM, which is quite low. Therefore, better docking was observed for the 3D02 protein than for the selected proteins with the M6-QE molecule. The O atom in the methoxy group and the N atom of the M6-QE molecule approached the H atoms of the THR 266 and HIS 166 residues of the 3D02 protein at a distance of 2.00 and 2.17 Å, respectively, and made conventional hydrogen bonds. Similarly,

the distance between the LYS 92 and VAL 93 residues of the 4OZ5 protein and the N atoms is 2.34 and 2.11, respectively. There is a conventional hydrogen bond between them. In the literature, there is an opinion that if there is a distance of around 2 Å between the ligand and the protein, there is very good docking.[64] According to the results obtained, we can say that there is good docking between the M6-QE molecule and the selected proteins and have confirmed the activity they have experimentally shown against these microorganisms by molecular docking studies.

Conclusion

The title molecule, M6-QE was subjected to experimental spectroscopic studies such as FT-IR, FT-Ra, and NMR (1H and 13 C), and its optimized molecular structure was obtained by DFT/B3LYP method at the level of 6–311++(d,p). The calculated geometric values are in good agreement with the experimental values. The HOMO-LUMO energy gap was calculated as 4.61 eV. It can be said that the title molecule has high chemical stability and reactivity. The MEP was traced, and chemical activity of the title molecule was noticed. The NLO properties were studied, and the calculated value of the first-order hyperpolarizability (β_{tot}) was found to be five times greater than the urea molecule. According to this result, the title molecule has the potential to be used as an NLO material. The thermodynamic properties were calculated, and their values, except Gibbs free energy values, were increasing with the increase in temperature. This increase in thermodynamic functions reveals that the title molecule has greater stability. This increase in thermodynamic functions reveals that the title molecule has greater stability. M6-QE is found to have strong antimicrobial activity against *A. hydrophila*, *S. dysenteriae*, *S. aureus*, *K. pneumoniae*, and *B. subtilis*. The title molecule also demonstrated strong anti-QS activity. The finding suggests that M6-QE has antimicrobial and anti-QS properties and that new powerful antimicrobial drugs may be useful in the treatment of the bacteria resistant to bacterial infections in the future. The M6-QE molecule is docked to the reactive regions of the 3D02 and 4OZ5 proteins with binding energies of −7.14 and −5.23 kcal/mol, respectively. According to the results obtained, we can say that there is good docking between the M6-QE molecule and the selected proteins and have confirmed the activity they have experimentally shown against these microorganisms by molecular docking studies.

CRediT authorship contribution statement

Senay Yurdakul: Supervision, conceptualization, reviewing, and editing

Merve Nurhan Güney: Software, material preparation, data collection, writing

Belgin Erdem: Antimicrobial analysis.

Disclosure statement

No potential conflict of interest was reported by the authors.

References

[1] Wallesch, M.; Nieger, M.; Volz, D.; Bräse, S. Copper (I) Complexes of 8-(diphenylphosphanyl-oxy)-quinoline: Photophysics, Structures and Reactivity. *Inorg. Chem. Commun.* **2017**, *86*, 232–240. DOI: 10.1016/j.inoche.2017.10.012.

[2] Matada, B. S.; Pattanashettar, R.; Yernale, N. G. A Comprehensive Review on the Biological Interest of Quinoline and its Derivatives. *Bioorg. Med. Chem.* **2021**, *32*, 115973. DOI: 10.1016/j.bmc.2021.116098.

[3] Shinde, P.; Pandharipande, S.; Thejokalyani, N.; Dhoble, S. J. Exploration of Photophysical Properties of Green Light Emitting Bis (8-hydroxyquinoline) Zinc (Znq2) Metal Chelate Under Various Environments. *Optik* **2018**, *162*, 151–160. DOI: 10.1016/j.ijleo.2018.02.075.

[4] Zhang, B.; Liu, H.; Wu, F.; Hao, G.; Chen, Y.; Tan, C.; Tan, Y.; Jiang, Y. A Dual-response Quinoline-based Fluorescent Sensor for the Detection of Copper (II) and Iron (III) Ions in Aqueous Medium. *Sens. Actuat. B Chem.* **2017**, *243*, 765–774. DOI: 10.1016/j.snb.2016.12.067.

[5] Geddes, C. D.; Douglas, P.; Moore, C. P.; Wear, T. J.; Egerton, P. L. Optical Thin-film Sensors for the Determination of Aqueous Halide Ions. *J. Fluorescence* **1999**, *9*(3), 163–171. DOI: 10.1023/A:1022502131091.

[6] van Staden, J. F.; Stefan, R. I. Simultaneous Flow Injection of Calcium, and Fluoride in Natural and Borehole Water with Conventional Ion-selective

Electrods in Series. *Talanta* **1999**, *49*(5), 1017–1022. DOI: 10.1016/S0039-9140(99)00060-0.

[7] Michalke, B.; Schramel, P.; Hasse, S. Determination of Free Iodide in Human Serum: Separation from Other I-species and Quantification in Serum Pools and Individual Samples. *Mikrochim. Acta* **1996**, *122*(1–2), 67–76. DOI: 10.1007/BF01252407.

[8] Poortvliet, L. J.; Horwitz, W. Determination of Chloride Concentration in Cheese: Collaborative Study. *J. AOAC Int.* **1982**, *65*(6), 1350–1356. DOI: 10.1093/jaoac/65.6.1350.

[9] Overman, R. F. Potentiometric Titration of Mercury Using the Iodide-selective Electrode as Indicator. *Anal. Chem.* **1971**, *43*(4), 616–617. DOI: 10.1021/ac60299a035.

[10] Martirosyan, A. R.; Rahim-Bata, R.; Freeman, A. B.; Clarke, C. D.; Howard, R. L.; Strobl, J. S. Differentiation-inducing Quinolines as Experimental Breast Cancer Agents in the MCF-7 Human Breast Cancer Cell Model. *Biochem. Pharmacol.* **2004**, *68*(9), 1729–1738. DOI: 10.1016/j.bcp.2004.05.003.

[11] Lee, H.-Y.; Nepali, K.; Huang, F.-I.; Chang, C.-Y.; Lai, M.-J.; Li, Y.-H.; Huang, H.-L.; Yang, C.-R.; Liou, J.-P. (N-Hydroxycarbonylbenylamino) Quinolines as Selective Histone Deacetylase 6 Inhibitors Suppress Growth of Multiple Myeloma In Vitro and In Vivo. *J. Med. Chem.* **2018**, *61*(3), 905–917. DOI: 10.1021/acs.jmedchem.7b01404.

[12] Mitscher, L. A. Bacterial Topoisomerase Inhibitors: Quinolone and Pyridone Antibacterial Agents. *Chem. Rev.* **2005**, *105*(2), 559–592. DOI: 10.1021/cr030101q.

[13] Fisher, L. M.; Pan, X. S. Methods to Assay Inhibitors of DNA Gyrase and Topoisomerase IV Activities. In *New Antibiotic Targets*; Humana Press: Totowa, NJ, 2008; pp. 11–23.

[14] Rashdan, H. R. M.; Abdelmonsef, A. H.; Abou-Krisha, M. M.; Yousef, T. A. Synthesis, Identification, Computer-Aided Docking Studies, and ADMET Prediction of Novel Benzimidazo-1,2,3-triazole Based Molecules as Potential Antimicrobial Agents. *Molecules (Basel, Switzerland)* **2021**, *26*(23), 7119. DOI: 10.3390/molecules26237119.

[15] Frisch, M.; Trucks, G.; Schlegel, H.; Scuseria, H.; Robb, M.; Cheeseman, J.; Scalmani, G.; Barone, V.; Mennucci, B.; Petersson, G. *Gaussian 09, Revision C. 01*; Gaussian, Inc.: Wallingford CT, 2009.

[16] Dennington, R.; Keith, T.; Millam, J. *GaussView, Version 5*; Semichem Inc.: Shawnee Mission, KS, 2009.

[17] Becke, A. D. A. New Mixing of Hartree–Fock and Local Density-functional Theories. *J. Chem. Phys.* **1993**, *98*(2), 1372–1377. DOI: 10.1063/1.464304.

[18] Lee, C.; Yang, W.; Parr, R. G. Development of the Colle-Salvetti Correlation-energy Formula into a Functional of the Electron Density. *Phys. Rev. B Condensed Matter.* **1988**, *37*(2), 785–789. DOI: 10.1103/PhysRevB.37.785.

[19] Balachandran, V.; Rajeswari, S.; Lalitha, S. Thermal and Magnetic Properties and Vibrational Analysis of 4-(dimethylamino) Pyridine: A Quantum Chemical Approach. *Spectrochim. Acta A Mol. Biomol. Spectrosc.* **2014**, *124*, 277–284. DOI: 10.1016/j.saa.2014.01.023.

[20] Merrick, J. P.; Moran, D.; Radom, L. An Evaluation of Harmonic Vibrational Frequency Scale Factors. *J. Phys. Chem. A* **2007**, *111*(45), 11683–11700. DOI: 10.1021/jp073974n.

[21] Lu, T.; Chen, F. Multiwfn: A Multifunctional Wavefunction Analyzer. *J. Comput. Chem.* **2012**, *33*(5), 580–592. DOI: 10.1021/jp073974n.

[22] Trott, O.; Olson, A. J.; Software, N. Update AutoDock Vina: Improving the Speed and Accuracy of Docking with a New Scoring Function, Efficient Optimization, and Multithreading. *J. Comput. Chem.* **2010**, *31*(2), 455–461. DOI: 10.1002/jcc.21334.

[23] Morris, G. M.; Goodsell, D. S.; Halliday, R. S.; Huey, R.; Hart, W. E.; Belew, R. K.; Olson, A. J. Automated Docking Using a Lamarckian Genetic Algorithm and an Empirical Binding Free Energy Function. *J. Comput. Chem.* **1998**, *19*(14), 1639–1662. DOI: 10.1002/(SICI)1096-987X(19981115)19:14<1639::AID-JCC10>3.0.CO;2-B.

[24] RSCB PDB Protein Data Bank. https://www.rcsb.org.

[25] https://www.3ds.com/products-services/biovia/products/molecular-modeling-simulation/biovia-discovery-studio.

[26] McClean, K. H.; Winson, M. K.; Fish, L.; Taylor, A.; Chhabra, S. R.; Camara, M.; Daykin, M.; Lamb, J. H.; Swift, S.; Bycroft, B. W.; et al. Quorum Sensing and Chromobacterium Violaceum: Exploitation of Violacein Production and Inhibition for the Detection of N-acylhomoserine Lactones. *Microbiology (Reading, England)* **1997**, *143 (Pt 12)*(12), 3703–3711. DOI: 10.1099/00221287-143-12-3703.

[27] CLSI. CLSI Supplement M100. In *Performance Standards for Antimicrobial Susceptibility Testing*, 28th ed.; Clinical and Laboratory Standards Institute: Wayne, PA, 2018.

[28] Gemiarto, A. T.; Ninyio, N. N.; Lee, S. W.; Logis, J.; Fatima, A.; Chan, E. W.; Lim, C. S. Isoprenyl Caffeate, a Major Compound in Manuka Propolis, is a Quorum-sensing Inhibitor in Chromobacterium Violaceum. *Antonie Van Leeuwenhoek* **2015**, *108*(2), 491–504. DOI: 10.1007/s10482-015-0503-6.

[29] Ravindranath, L.; Reddy, B. V. Theoretical and Experimental Study of Torsional Potentials, Molecular Structure (Monomer and Dimer), Vibrational Analysis and Molecular Characteristics of Some Dimethyl Bipyridines. *J. Mol. Struct.* **2020**, *1200*, 127089. DOI: 10.1016/j.molstruc.2019.127089.

[30] Kucuk, C.; Yurdakul, S.; Erdem, B. Experimental and Theoretical Fourier Transform Infrared and Raman Spectroscopy, Density Functional Theory,

Antibacterial Activity and Molecular Docking Studies on 1-(4-methoxyphenyl)-1H-imidazole. *Chem. Papers* **2022**, *76*(5), 2833–2854. DOI: 10.1007/s11696-021-02017-8.

[31] Moreno-Fuquen, R.; Hernandez, G.; Kennedy, A. R.; Morrison, C. A. Supramolecular Study, Hirshfeld Analysis and Theoretical Study of 6-methoxyquinoline N-oxide Dihydrate. *Acta Crystallograph. Sect. C Crystal Struct. Commun.* **2013**, *69*(Pt 6), 665–670. DOI: 10.1107/S0108270113011979.

[32] Govindarajan, M.; Ganasan, K.; Periandy, S.; Karabacak, M.; Mohan, S. Vibrational Spectroscopic Analysis of 2-chlorotoluene and 2-bromotoluene: A Combined Experimental and Theoretical Study. *Spectrochim. Acta A Mol. Biomol. Spectrosc.* **2010**, *77*(5), 1005–1013. DOI: 10.1016/j.saa.2010.08.038.

[33] Saleem, H.; Krishnan, A. R.; Erdogdu, Y.; Subashchandrabose, S.; Thanikachalam, V.; Manikandan, G. Density Functional Theory Studies on 2, 5-bis (4-hydroxy-3-methoxybenzylidene) Cyclopentanone. *J. Mol. Struct.* **2011**, *999*(1–3), 2–9. DOI: 10.1016/j.molstruc.2011.02.039.

[34] Sarıkaya, E. K.; Dereli, Ö. Molecular Structure and Vibrational Spectra of 7-Methoxy-4-methylcoumarin by Density Functional Method. *J. Mol. Struct.* **2013**, *1052*, 214–220. DOI: 10.1016/j.molstruc.2013.08.024.

[35] Sureshkumar, B.; Mary, Y. S.; Resmi, K. S.; Panicker, C. Y.; Yohannan, C.; Armaković, S.; Armaković, S. J.; Van Alsenoy, C.; Narayana, B.; Suma, S. Spectroscopic Analysis of 8-hydroxyquinoline Derivatives and Investigation of its Reactive Properties by DFT and Molecular Dynamics Simulations. *J. Mol. Struct.* **2018**, *1156*, 336–347. DOI: 10.1016/j.molstruc.2017.11.120.

[36] Celik, S.; Alp, M.; Yurdakul, S. A Combined Experimental and Theoretical Study on Vibrational Spectra of 3-pyridyl Methyl Ketone. *Spectrosc. Lett.* **2020**, *53*(4), 234–248. DOI: 10.1080/00387010.2020.1734840.

[37] Badoğlu, S.; Yurdakul, Ş. An Experimental Vibrational Spectroscopic and Density Functional Theory Computational Study on 2, 4-dioxopyrimidine in Solvation Phase. *Int. J. Quant. Chem.* **2023**, *123*(8), e27073. DOI: 10.1002/qua.27073.

[38] Srivastava, S.; Gupta, P.; Sethi, A.; Pratap, S. R. One Pot Synthesis of Curcumin NSAIDs Prodrug, Spectroscopic Characterization, Conformational, Analysis, Chemical Reactivity, Intramolecular Interactions and First Order Hyperpolarizability by DFT Method. *J. Mol. Struct.* **2016**, *1117*, 173–180. DOI: 10.1016/j.molstruc.2016.03.033.

[39] Pereira, FF; Xiao, K.; Latino, D. A.; Wu, C.; Zhang, Q.; Aires-de-Sousa, J. Machine Learning Methods to Predict Density Functional Theory B3LYP Energies of HOMO and LUMO Orbitals. *J. Chem. Inform. Model.* **2017**, *57*(1), 11–21. DOI: 10.1021/acs.jcim.6b00340.

[40] Rocha, M.; Di Santo, A.; Arias, J. M.; Gil, D. M.; Ben Altabef, A. Ab-initio and DFT Calculations on Molecular Structure, NBO, HOMO–LUMO Study and a New Vibrational Analysis of 4-(dimethylamino) Benzaldehyde. *Spectrochim. Acta A Mol. Biomol. Spectrosc.* **2015**, *136 Pt B*, 635–643. DOI: 10.1016/j.saa.2014.09.077.

[41] Xavier, S.; Periandy, S.; Carthigayan, K.; Sebastian, S. Molecular Docking, TG/DTA, Molecular Structure, Harmonic Vibrational Frequencies, Natural Bond Orbital and TD-DFT Analysis of Diphenyl Carbonate by DFT Approach. *J. Mol. Struct.* **2016**, *1125*, 204–216. DOI: 10.1016/j.molstruc.2016.06.071.

[42] Balachandran, V.; Murugan, M.; Karpagam, V.; Karnan, M.; Ilango, G. Conformational Stability, Spectroscopic (FT-IR & FT-Raman), HOMO–LUMO, NBO and Thermodynamic Function of 4-(trifloromethoxy) Phenol. *Spectrochim. Acta A Mol. Biomol. Spectrosc.* **2014**, *130*, 367–375. DOI: 10.1016/j.saa.2014.04.043.

[43] Hellal, A.; Rachida, D.; Zaout, S.; Elkolli, M.; Chafaa, S.; Touafri, L.; Chafai, N.; Mehri, M.; Benbougerra, K. Structural, Electronic, Vibrational, Optical and Thermodynamic Properties of 3-Oxo-3-p-tolylpropylphosphonic Acid and 4-Oxo-4-p-tolyl-butyric Acid: Density Functional Theory Study. *J. Mol. Struct.* **2018**, *1171*, 527–540. DOI: 10.1016/j.molstruc.2018.06.012.

[44] Raajaraman, B. R.; Sheela, N. R.; Muthu, S. Spectroscopic, Quantum Computational and Molecular Docking Studies on 1-phenylcyclopentane Carboxylic Acid. *Comput. Biol. Chem.* **2019**, *82*, 44–56. DOI: 10.1016/j.compbiolchem.2019.05.011.

[45] Bultinck, P.; Carbó-Dorca, R.; Langenaeker, W. Negative Fukui Functions: New Insights Based on Electronegativity Equalization. *J. Chem. Phys.* **2003**, *118*(10), 4349–4356. DOI: 10.1063/1.1542875.

[46] Yang, W.; Mortier, W. J. The Use of Global and Local Molecular Parameters for the Analysis of the Gas-phase Basicity of Amines. *J. Am. Chem. Soc.* **1986**, *108*(19), 5708–5711. DOI: 10.1021/ja00279a008.

[47] Parr, R. G.; Yang, W. T. Density Functional Approach to the Frontier-electron Theory of Chemical Reactivity. *J. Am. Chem. Soc.* **1984**, *106*(14), 4049–4050. DOI: 10.1021/ja00326a036.

[48] Roy, R. K.; Krishnamurti, S.; Geerlings, P.; Pal, S. Local Softness and Hardness Based Reactivity Descriptors for Predicting Intra-and intermolecular Reactivity Sequences: Carbonyl Compounds. *J. Phys. Chem. A* **1998**, *102*(21), 3746–3755. DOI: 10.1021/jp973450v.

[49] Halim, S. A.; Abdel Rahman, M. A. First Principles Density Functional Theoretical Study on the Structures, Reactivity and Spectroscopic Properties of (NH) and (OH) Tautomer's of 4(methylsulfanyl) 3[(1Z)1 (2phenylhydrazinylidene) ethyl] Quinoline2(1H)one. *Sci. Rep.* **2023**, *13*(1), 8909. DOI: 10.1038/s41598-023-35933-8.

[50] Cramer, C. H. *Essentials of Computational Chemistry: Theories and Models*; John Wiley & Sons LTD: Chichester, 2002.

[51] Kleinman, D. A. Nonlinear Dielectric Polarization in Optical Media. *Phys. Rev.* **1962**, *126*(6), 1977–1979. DOI: 10.1103/PhysRev.126.1977.

[52] Sajan, D.; Joe, H.; Jayakumar, V. S.; Zaleski, J. Structural and Electronic Contributions to Hyperpolarizability in Methyl P-hydroxy Benzoate. *J. Mol. Struct.* **2006**, *785*(1–3), 43–53. DOI: 10.1016/j.molstruc.2005.09.041.

[53] Sethi, A.; Singh, R. P.; Shukla, D.; Singh, P. Synthesis of Novel Pregnane-Diosgenin Prodrugs via Ring a and Ring a Connection: A Combined Experimental and Theoretical Studies. *J. Mol. Struct.* **2016**, *1125*, 616–623. DOI: 10.1016/j.molstruc.2016.07.020.

[54] Büyükmurat, Y.; Akyüz, S. Theoretical and Experimental IR Spectra and Assignments of 3-Aminopyridine. *J. Mol. Struct.* **2001**, *563–564*, 545–550. DOI: 10.1016/S0022-2860(00)00801-2.

[55] Singh, P.; Islam, S. S.; H. Ahmad, H.; Prabaharan, A. Spectroscopic Investigation (FT-IR, FT-Raman), HOMO-LUMO, NBO, and Molecular Docking Analysis of N-ethyl-N-nitrosourea, a Potential Anticancer Agent. *J. Mol. Struct.* **2018**, *1154*, 39–50. DOI: 10.1016/j.molstruc.2017.10.012.

[56] Yurdakul, S.; Temel, E.; Büyükgüngör, O. Crystal Structure, Spectroscopic Characterization, Thermal Properties and Theoretical Investigations on [Ag (methyl 4-pyridyl ketone) 2NO3]. *J. Mol. Struct.* **2019**, *1191*, 301–313. DOI: 10.1016/j.molstruc.2019.04.071.

[57] Steinmann, S. N.; Mo, Y.; Corminboeuf, C. How Do Electron Localization Functions Describe π-electron Delocalization. *Phys. Chem. Chem. Phys.* **2011**, *13*(46), 20584–20592. DOI: 10.1039/c1cp21055f.

[58] Fuentealba, P.; Chamorro, E.; Santos, J. C. Understanding and Using the Electron Localization Function. In *Theoretical and Computational Chemistry*; Elsevier: Amsterdam, Netherlands, 2007; Vol. 19, pp. 57–85.

[59] Senerovic, L.; Opsenica, D.; Moric, I.; Aleksic, I.; Spasić, M.; Vasiljevic, B. Quinolines and Quinolones as Antibacterial, Antifungal, Anti-virulence, Antiviral and Anti-parasitic Agents. *Adv. Microbiol. Infect. Dis. Public Health* **2020**, *14*, 37–69.DOI: 10.1007/5584.2019.428

[60] Defoirdt, T. Quorum-sensing Systems as Targets for Antivirulence Therapy. *Trend. Microbiol.* **2018**, *26*(4), 313–328. DOI: 10.1016/j.tim.2017.10.005.

[61] Albuquerque, P.; Casadevall, A. Quorum Sensing in Fungi–a Review. *Med. Mycol.* **2012**, *50*(4), 337–345. DOI: 10.3109/13693786.2011.652201.

[62] Amul, B.; Muthu, S.; Raja, M.; Sevvanthi, S. Spectral, DFT and Molecular Docking Investigations on Etodolac. *J. Mol. Struct.* **2019**, *1195*, 747–761. DOI: 10.1016/j.molstruc.2019.06.047.

[63] Kucuk, C.; Celik, S.; Yurdakul, S.; Coteli, E. An Experimental and Computational Studies, Evaluating the In Vitro Antidiabetic and Antioxidant Activity, In Silico Prediction ADMET Properties of 5-chloro-1H-benzimidazole and its Newly Synthesized Silver (I) Complex. *Appl. Organometall. Chem.* **2024**, *38*(6), e7499. DOI: 10.1002/aoc.7499.

[64] Kucuk, C. Synthesis, Characterization, DFT Studies, and Molecular Docking Investigation of Silver Nitrate Complex of 5-benzimidazole Carboxylic Acid as Targeted Anticancer Agents. *J. Mol. Struct.* **2023**, *1293*, 136166. DOI: 10.1016/j.molstruc.2023.136166.

[65] Erdogdu, Y.; Unsalan, O.; Sajan, D.; Gulluoglu, M. T. Structural Conformations and Vibrational Spectral Study of Chloroflavone with Density Functional Theoretical Simulations. *Spectrochim. Acta. A Mol. Biomol. Spectrosc.* **2010**, *76*(2), 130–136. DOI: 10.1016/j.saa.2010.02.043.

[66] Zevallos, J.; Toro-Labbé, A. A Theoretical Analysis of the Kohn-Sham and Hartree-Fock Orbitals and their Use in the Determination of Electronic Poperties. *J. Chilean Chem. Soc.* **2003**, *48*(4), 39–47. DOI: 10.4067/S0717-97072003000400007.